Doctoral Dissertation (Censored)

博士論文 (要約)

Assessment of the finescale parameterizations of deep ocean mixing in the Antarctic Circumpolar Current region based on microstructure measurements and eikonal calculations

(南極周極流域における深海乱流パラメタリゼーションの有効性 -乱流直接観測と波追跡シミュレーションの結果から-)

A Dissertation Submitted for the Degree of Doctor of Philosophy

December 2019

令和元年 12 月博士 (理学) 申請

Department of Earth and Planetary Science,
Graduate School of Science,
The University of Tokyo

東京大学理学系研究科地球惑星科学専攻

Anne Takahashi

髙橋　杏

Abstract

The Southern Ocean is a special place where the Antarctic Circumpolar Current (ACC), the bottom-reaching geostrophic flow accompanying vigorous eddies, coexists with the energetic internal waves: near-inertial internal waves generated by strong atmospheric disturbances and internal lee waves generated by the ACC impinging on the small scale bottom topographic features. Breaking of these internal waves is considered to provide strong turbulent mixing. Although quantification of diapycnal mixing in the Southern Ocean has been considered to be important for better understanding of the global meridional overturning circulation (MOC), the number of direct microstructure measurements is limited, and the intensity of turbulent mixing has been commonly estimated using finescale parameterizations.

However, it has been reported that the existing finescale parameterizations tend to overestimate the actual turbulent dissipation rates in the ACC region. This suggests that the finescale parameterizations, which are formulated on the basis of the wave-wave interactions within the background internal wave field, do not grasp the turbulent mixing processes in the ACC region. In this dissertation, on the basis of the field observations and numerical simulations called "eikonal calculations", we investigate why the finescale parameterizations cannot accurately estimate the turbulent dissipation rates in the ACC region for clarifying turbulent mixing processes there.

First of all, we find that the most plausible reason for the overestimating tendency of the finescale parameterizations is that the vertical wave number spectrum of the internal wave energy is distorted from the canonical Garrett-Munk (GM) spectrum and has a spectral "hump" in lower vertical wave numbers. Our eikonal calculations show that the low vertical wave number internal wave packets constituting the hump hardly cascade down to the turbulent scales, because their vertical scales are much larger than the scales of breaking

waves. The existing finescale parameterizations assume that the background internal wave field has a GM-like flat-shaped vertical wave number energy spectrum. Then, the turbulent dissipation rates are estimated from the finescale shear and strain spectral levels, which are calculated by integrating the shear and strain spectra from the lowest wave number to the cut-off wave number. When we apply the finescale parameterizations to the observed velocity profiles, this cut-off wave number is normally set to a smaller value because the shear spectra tend to be contaminated by noise at higher wave numbers. Therefore, the estimated shear and strain spectral levels become much larger than the spectral level at higher wave numbers, which explains the observed bad performance of the finescale parameterizations.

On the other hand, the previous research theoretically speculated that the wave-mean flow interactions between internal lee waves and geostrophic shear flows might be the cause of the overestimating tendency of the finescale parameterizations. This hypothesis, however, is not supported by our eikonal calculations showing that in the realistic situation where the background mean flow shear and internal wave field coexist, the finescale parameterizations would rather underestimate the actual turbulent dissipation rates.

"Humps" in the finescale spectra might be created by low vertical wave number near-inertial wave or internal lee wave packets superposed on a GM-like internal wave field. From multivariate correlation analyses of the field observation data, it is suggested that these internal wave packets are generated or amplified by large scale geostrophic shear flows. In our eikonal calculations, low vertical wave number internal wave packets promote the breaking of high vertical wave number internal waves, resulting in enhanced turbulent mixing. Therefore, geostrophic shear flows might contribute indirectly to the enhanced turbulent mixing in the Southern Ocean. These pictures are quite different from the conventional interpretation of the turbulent mixing in the ACC region, where the breaking of the near-inertial and internal lee waves as well as the wave-mean flow interaction between these internal waves and the ACC are considered to play important roles.

Contents

1 General Introduction **4**

1.1 Meridional overturning circulation 4

1.2 Diapycnal and isopycnal mixing in the Southern Ocean 5

1.3 Finescale parameterization of deep ocean mixing 9

1.4 Overview of this dissertation 11

2 Microstructure Measurements in the Antarctic Circumpolar Current (ACC) Region **18**

2.1 Introduction 18

2.2 Data and analysis 20

2.2.1 Data 20

2.2.2 Microstructure analysis 21

2.2.3 Finestructure analysis 22

2.2.4 Application of finescale parameterizations 23

2.3 Results 28

2.4 Concluding remarks 28

Appendix 2.A Derivation and interpretation of the rotary coefficient 33

2.A.1 Derivation of the rotary component spectra 33

2.A.2 Interpretation of the rotary coefficient 35

2.A.3 Definition of the rotary coefficient 36

3 Eikonal Calculations I : Influence of the Distortion of the Internal Wave Spectrum 38

3.1 Introduction 38

3.2 Eikonal calculations 39

3.3 Standard experiment 39

3.4 Hump experiments 39

3.5 Conclusions and discussions 39

Appendix 3.A Background velocity field of the Garrett-Munk (GM) spectrum 40

Appendix 3.B Background velocity field for the hump experiments 40

4 Eikonal Calculations II : Influence of the Large Scale Mean Flow Shear 41

4.1 Introduction 41

4.2 Hypothesis in Waterman et al. (2014) 42

4.3 Lee wave packet experiments 44

4.4 Spectrum experiments 44

4.5 Concluding remarks 44

5 General Conclusion 47

5.1 Summary of this dissertation 47

5.1.1 Assessment of the finescale parameterizations in the ACC region . 48

5.1.2 The role of geostrophic shear in the breaking of internal waves . . 49

5.1.3 Turbulent mixing processes in the ACC region 50

5.1.4 Significance of this study 51

5.2 Discussions and future works 51

5.2.1 Applicability of the present results to the Kuroshio region 52

5.2.2 Climatology of the background GM-like internal wave spectrum . 52

5.2.3 For further improvements of the finescale parameterization 54

5.2.4 Implications for parameterizations of internal lee wave-driven mixing in ocean general circulation models 55

Acknowledgement **58**

References **60**

Chapter 1

General Introduction

1.1 Meridional overturning circulation

The meridional overturning circulation (MOC) plays an important role in maintaining the mild climate of the earth, and this MOC is thought to have a significant influence on the long-term climate change by transporting heat, fresh water, and carbon. The starting point of the MOC is the deep water formation with deep convection in the polar oceans such as the Labrador Sea, the Greenland-Iceland Sea in the northern North Atlantic, and the Weddell Sea, and the Ross Sea around Antarctica. These dense waters should rise somewhere and ultimately flow back to the sinking regions to close the circulation. However, the detailed upwelling pathways of the overturning cells have not yet been clarified.

It is well known that the strength and structure of the MOC strongly depend on the global distribution of diapycnal mixing (Bryan 1987; Tsujino et al. 2000), which is mainly caused by breaking of oceanic internal waves. Munk and Wunsch (1998) estimated that 2.1 TW (1 TW = 10^{12} W) of the internal wave energy is required to maintain the global abyssal density stratification against 30 Sverdrups of deep water formation. The main sources of internal wave energy that provide diapycnal mixing have been considered to be tidal flows interacting with bottom topographic features and winds acting on the mixed layer to generate near-inertial internal waves.

Niwa and Hibiya (2011) investigated the spatial distribution of the diapycnal diffusivity due to the dissipation of major semidiurnal (M_2 and S_2) and diurnal (K_1 and O_1) baroclinic tide energy (Figure 1.1) using a three-dimensional high resolution primitive equation

model incorporating realistic bottom topography, density stratification, and barotropic tidal forcing. They found that global barotropic tidal energy is converted into 1.1 TW of baroclinic tide energy over the prominent topographic features, but only 45 – 55 % (0.5 – 0.6 TW) of its energy is dissipated below a depth of 1000 m and available for deep ocean mixing.

Furuichi et al. (2008) examined the global distribution of the wind-induced near-inertial wave energy using a three-dimensional primitive equation model. In their simulation, the annual mean of the global wind energy input into surface near-inertial motions is $\sim$ 0.4 TW, but 75 – 85 % of its energy is dissipated in the surface 150 m because a large part of wind induced energy resides in high vertical modes that are subject to local dissipation in the upper ocean. As a result, the total energy of the wind-induced near-inertial waves available for deep ocean mixing is estimated to be, at most, 0.1 TW. It should be noted that, however, Rimac et al. (2013) pointed out that the estimates of the wind power input to near-inertial motions strongly depends on the temporal and spatial resolution of the wind stress data products.

These baroclinic tide energy (0.6 TW) and near-inertial wave energy (0.1 TW) available for deep ocean mixing seem to be insufficient to sustain the MOC (2.1 TW). This "missing mixing" paradox has been controversial in oceanographic literature. Recently, as a key to solving this paradox, physical processes in the Southern Ocean is attracting attentions.

1.2 Diapycnal and isopycnal mixing in the Southern Ocean

In the Southern Ocean, the strong westerly wind drives the Antarctic Circumpolar Current (ACC), which is the largest current in the global ocean. Multiple jets of the ACC flow eastward between 40°S and 65°S around the globe, without blocked by continents (Figure 1.2).

One of the special characteristics of the ACC is that the flows extend to great depth. Due to its high latitude, weak stratification, and strong eastward flow, baroclinic Rossby

waves cannot propagate to the west in the ACC, which inhibits the geostrophic adjustment for developing a Sverdrup balance that limits the depth of wind-driven circulation at lower latitude (Hughes 2005; Rintoul 2018). Therefore, the ACC has an equivalent-barotropic structure thus can interact with the bottom topography, which makes it possible to excite internal lee waves in the Southern Ocean.

Internal lee waves, generated by quasi-steady geostrophic flows impinging on small scale topographic features, are thought to be one of the major sink of the wind energy input to the ocean general circulation (e.g., Nikurashin et al. 2013). Nikurashin and Ferrari (2011) estimated the global distribution of generation rates of the internal lee waves by applying a linear theory to bottom topographic spectra estimated from single beam echo soundings, climatological bottom stratification, and bottom velocity taken from a global ocean model. They found that the energy flux into bottom-generated internal lee waves is estimated to be 0.1 TW in the Southern Ocean, which accounts for half of the global energy flux (0.2 TW) of internal lee waves (Figure 1.4). Recent numerical simulations using an ocean-ice-atmosphere coupled model suggested that, while the global energy input into internal lee waves is smaller than that into internal tides, lee wave-driven mixing has a significant impact on the ocean thermal structure and stratification, as well as on the MOC (Melet et al. 2014).

Another special characteristic of the ACC is that the flows accompany vigorous eddies. Strong westerly winds drive the northward Ekman transport with convergence (downwelling) north of the wind-stress maximum and divergence (upwelling) south of it (e.g., Rintoul 2018). This makes isopycnals to slope upwards to south, establishing the geostrophic balance of the ACC. The steeply sloping isopycnals are baroclinically unstable and form eddies (Olbers et al. 2004; Rintoul 2018), which might have smaller horizontal and vertical scales and might interact with internal waves.

The laterally sloping isopycnals of the ACC allow deep water to upwell quasi-adiabatically (along-isopycnally) to the sea surface. From a long time ago, the pattern

suggestive of a two-cell MOC (see Figure 1.3), which consists of an upper cell and a lower cell, has been revealed by hydrographic sections of temperature, salinity, oxygen, and many other tracers. In the upper cell of the MOC, North Atlantic Deep Water (NADW), which is generated through the deep water formation in the North Atlantic, flows southward along isopycnals and becomes Upper Circumpolar Deep Water (UCDW). Then, the UCDW outcrops at the sea surface within the ACC belt, where it is converted to lighter water and flows back equatorward by the Ekman transport. On the other hand, some of the NADW flows southward across the Southern Ocean and becomes Lower Circumpolar Deep Water (LCDW), which outcrops near Antarctica. The lower cell of the MOC is driven by the formation of the densest Antarctic Bottom Water (AABW) from the LCDW due to the surface cooling and brine rejection associated with sea ice generation. This wind-driven MOC in the Southern Ocean provides the deep water with a quasi-adiabatic route to the surface, which might resolve the missing mixing paradox (e.g., Speer et al. 2000; Webb and Suginohara 2001; Marshall and Speer 2012). It should be noted that, however, diapycnal mixing is still required to drive the lower cell of the MOC through the upward transport of water from the densest layer to mid-depths.

Although its potential importance had been pointed out, because of the harsh sea and weather condition of the ACC region, the distribution of diapycnal mixing in the Southern Ocean had been unknown until extensive microstructure measurements (St. Laurent et al. 2012; Waterman et al. 2013; Sheen et al. 2013) and tracer release experiments (Ledwell et al. 2011) were carried out since the 2000s. These observations revealed that the turbulent dissipation rates are enhanced in the upper $\sim$ 1000 m associated with downward-propagating near-inertial waves, which might be generated by strong atmospheric disturbances, and both the turbulent dissipation rates and the derived diapycnal diffusivities[1] are enhanced in the deep ocean (within $\sim$ 1000 m above bottom) with strong near-bottom flows and rough bottom topography, which strongly suggests that the breaking

[1]The diapycnal diffusivity K_ρ is estimated using the Osborn relation, $K_\rho = \Gamma \varepsilon N^{-2}$ (Osborn 1980) with ε the observed turbulent dissipation rates, $\Gamma = 0.2$ the mixing efficiency, and N^2 the stratification.

of internal lee waves contributes to the strong mixing.

Extensive measurements of the internal wave field using high-resolution autonomous profiling floats, which obtain a lot of vertical profiles of horizontal velocity, conductivity, and temperature along their trajectories (Meyer et al. 2015, 2016), revealed that the internal wave characteristics and the diapycnal diffusivities estimated using the finescale parameterization (Gregg et al. 2003; Henyey et al. 1986; Polzin et al. 1995) have large spatial and temporal variability. Meyer et al. (2015) summarized the dynamics of diapycnal mixing suggested by observations in the Kerguelen Plateau, a major topographic feature in the Southern Ocean (Figure 1.5). In the strong ACC frontal zones, mixing intensities are enhanced on the rough topographic features due to the generation and breaking of upward-propagating internal lee waves, which are also advected away from the generation sites. In the Subantarctic zone, stronger wind disturbances generate downward-propagating near-inertial waves, and enhanced mixing which might be associated with mesoscale eddies is also observed.

Although the understanding of diapycnal mixing in the Southern Ocean has greatly advanced by the recent extensive observations as well as numerical simulations, the distribution of diapycnal mixing has not yet been fully quantified because the number of microstructure measurements is still limited for capturing spatially patchy and temporally intermitted turbulent mixing. Due to the increasing number of the Argo profilers which have been deployed globally, the spatial distribution of the turbulent dissipation rates within 2000 m from the sea surface can be estimated by applying the finescale parameterization to the vertical profiles of density (Wu et al. 2011; Whalen et al. 2012). It has been pointed out, however, that the existing finescale parameterizations tend to overestimate the actual turbulent dissipation rates in the ACC region (Waterman et al. 2014; Takahashi and Hibiya 2019). This indicates that our understanding of the turbulent mixing processes in the Southern Ocean is still insufficient, and there might be some physical processes that are not considered in the existing finescale parameterizations. The finescale parameteri-

zations assume the turbulent mixing caused by energy cascades associated with nonlinear interactions in the background internal wave field. However, it is not fully clarified how the vigorous geostrophic shear flows including eddies associated with the ACC affects the breaking of internal waves.

1.3 Finescale parameterization of deep ocean mixing

Since direct measurements of microscale (< 1 m in vertical) turbulence are time consuming and require expensive instruments, finescale parameterizations of deep ocean mixing (Henyey et al. 1986; Gregg 1989; Wijesekera et al. 1993; Polzin et al. 1995; Gregg et al. 2003; Ijichi and Hibiya 2015), in which the turbulent dissipation rates are estimated in terms of finescale ($\sim$ 100 m in vertical) velocity and/or density profiles, have been developed.

These finescale parameterizations predict the turbulent dissipation rates as the internal wave energy flux that cascades down to the turbulent scales due to nonlinear interactions within the background internal wave spectrum (Figure 1.6). Furthermore, it is implicitly assumed that the background internal wave field is in a steady state, isotropic, and it has flat-shaped vertical wave number spectra of shear $\mathbf{u_z}$ and strain[2] ξ_z, like the universal internal wave spectrum model known as the Garrett-Munk (GM) spectrum (Garrett and Munk 1972, 1975; Cairns and Williams 1976; Munk 1981). The internal wave energy spectrum of the GM model is expressed in a variable separation form for frequency σ and vertical wave number m such that,

$$\Phi_E^{GM}(\sigma, m) = b^2 N_0 N E_{GM} \Omega_{GM}(\sigma) M(m), \tag{1.1}$$

where $b = 1300$ m, $N_0 = 5.2 \times 10^{-3}$ rad/s, and $E_{GM} = 6.3 \times 10^{-5}$ are constant coefficients, and N is the buoyancy frequency. It should be noted that this GM spectrum, which was

[2]Strain ξ_z is the vertical gradient of the vertical displacement of the isopycnals.

formulated based on the observations from site D in the western North Atlantic (Garrett and Munk 1972), has been used as the first order approximation of the background internal wave field in the interior ocean, though it has been found that the internal wave spectrum is more or less distorted from the GM model in many regions (e.g. Polzin and Lvov 2011).

The pioneering research (Gregg 1989; Wijesekera et al. 1993) proposed the prototype of the finescale parameterizations based on the theoretical model of the spectral energy transfer provided by Henyey et al. (1986). They assumed that the background internal wave spectrum is similar to the GM spectrum while changing its energy level E_{GM} in (1.1), which is estimated from either the shear spectral level (Gregg 1989) or strain spectral level (Wijesekera et al. 1993). After that, Polzin et al. (1995) considered the situation in which the frequency spectrum of the background internal wave field, namely, $\Omega_{GM}(\sigma)$ in (1.1) is distorted from the GM model, and they improved the above parameterizations by introducing a new parameter, shear/strain ratio R_ω. By adding a latitudinal dependent term (Gregg et al. 2003), this improved parameterization called the Gregg-Henyey-Pozin (GHP) parameterization has been widely used as the most reliable parameterization.

Hibiya et al. (2012) examined the validity of these finescale parameterizations near prominent topographic features in the North Pacific by comparing the turbulent dissipation rates estimated from each parameterization and those obtained from microstructure measurements. They found that the internal wave spectra were distorted from the GM spectrum in these regions, so that the shear-based (Gregg 1989) and strain-based (Wijesekera et al. 1993) parameterizations became erroneous but the GHP parameterization, which takes into account the frequency content of the internal wave field, could estimate the turbulent dissipation rates more accurately.

Recently, Ijichi and Hibiya (2015) pointed out the defect of the R_ω dependent term in the GHP parameterization to propose a revised parameterization. This Ijichi-Hibiya (IH) parameterization could predict the turbulent dissipation rates more accurately than the GHP parameterization in the Izu-Ogasawara Ridge where the internal wave frequency

spectra are significantly redder (biased to lower frequencies) than the GM spectrum (Ijichi and Hibiya 2015).

Although the finescale parameterizations have also been used in the Southern Ocean (e.g., Naveira-Garabato et al. 2004; Wu et al. 2011; Meyer et al. 2015), their validity in the Southern Ocean should be investigated because the finescale parameterizations are only concerned with the wave-wave interactions within the background internal wave field, so that they do not consider other physical processes such as those associated with geostrophic currents. In fact, it was reported from the results of microstructure measurements carried out in the Kerguelen Plateau (Waterman et al. 2013, 2014), the Drake Passage (Sheen et al. 2013), and south of Australia (Takahashi and Hibiya 2019) that the turbulent dissipation rates estimated using the finescale parameterizations tend to overestimate the microstructure-derived values by up to a factor of 10, in some region.

1.4 Overview of this dissertation

The main purpose of this dissertation is to elucidate the turbulent mixing processes in the ACC region where the internal wave field and geostrophic flows coexist. In particular, we focus on the problem that the existing finescale parameterizations of deep ocean mixing fail to predict the actual turbulent dissipation rates in the ACC region. Furthermore, we investigate the role of geostrophic shear in breaking of internal waves.

In Chapter 2, we examine the relationship between the characteristics of the finescale internal wave field and the microscale turbulent mixing in the ACC region using available dataset of the field observations carried out in the Southern Ocean. Here we confirm that the finescale parameterizations systematically overestimate the actual turbulent dissipation rates especially at the locations where the vertical wave number spectra of the internal wave energy are distorted from the canonical GM spectrum.

Motivated by this result, in Chapter 3, we carry out numerical simulations called "eikonal calculations" to quantitatively examine the turbulent mixing processes in such

distorted spectra. Since the results of numerical experiments, including the dependence of the parameters characterizing the internal wave field on the performance of the finescale parameterization, are consistent with the observation results, we propose the plausible reason why the finescale parameterization fails to predict the turbulent dissipation rates in the ACC region.

In Chapter 4, we explore another possibility, which was proposed by Waterman et al. (2014), that the wave-mean flow interaction between bottom-generated internal lee waves and background geostrophic shear flows associated with the ACC might be the cause of the observed discrepancy between the actual turbulent dissipation rates and those predicted by the finescale parameterization. In order to verify their hypothesis quantitatively, we carry out eikonal calculations and reproduce the propagation, refraction, and breaking of the bottom-generated internal lee wave packets incorporating not only the background mean flow shear but also the background internal wave field, the latter of which has not been considered in the previous studies (Waterman et al. 2014; Kunze and Lien 2019). Results of our numerical experiments suggest that their hypothesis becomes implausible in the existence of the background internal wave field.

In Chapter 5, we summarize this dissertation, discuss the obtained results from a broad perspective, and present our future prospects.

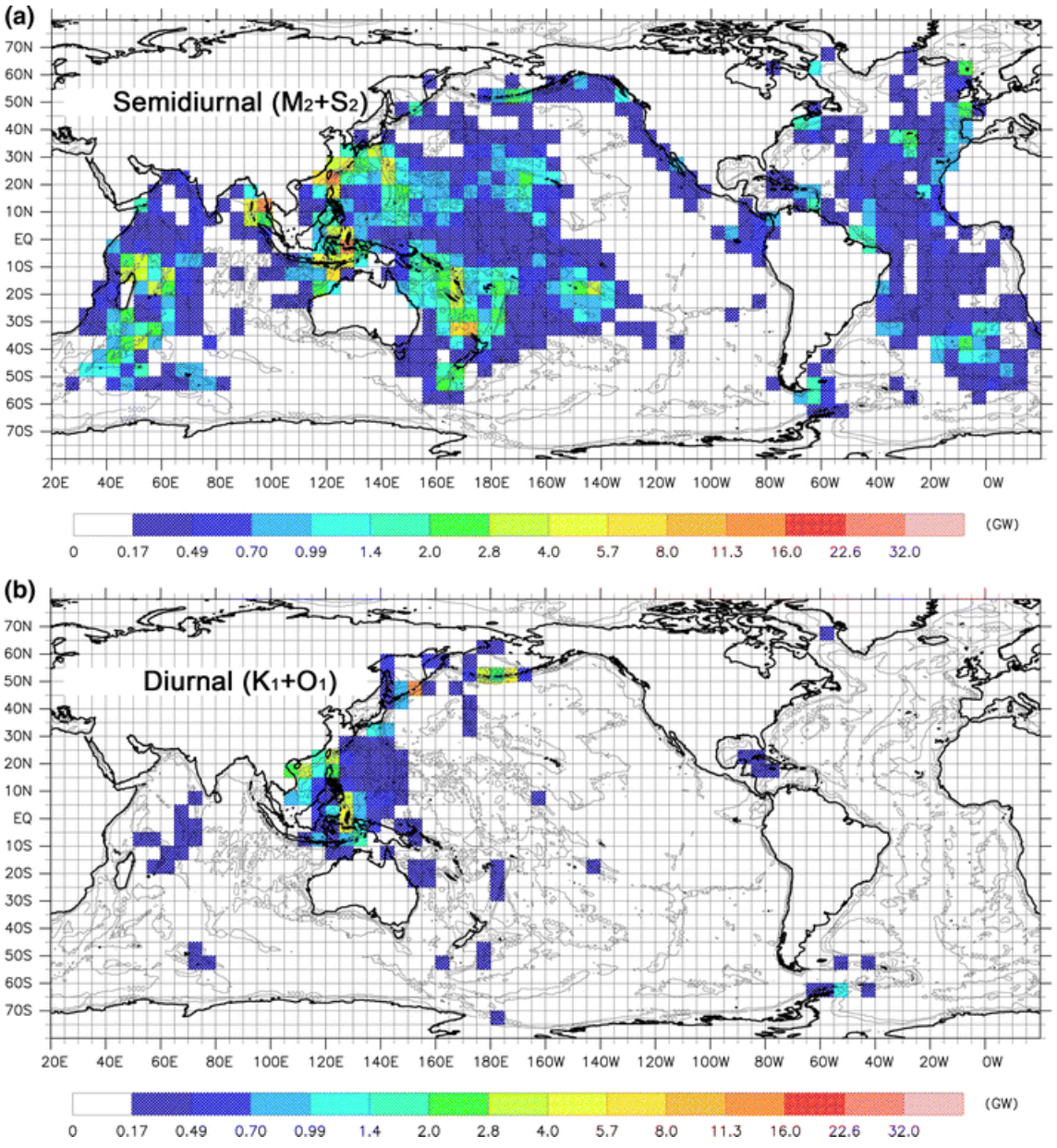

Figure 1.1: The depth-integrated dissipation rate of the baroclinic tide energy for the (a) semidiurnal (M_2 and S_2) and (b) diurnal (K_1 and O_1) tidal constituents. **© Reprinted by permission from Springer Nature: Niwa and Hibiya (2011)**

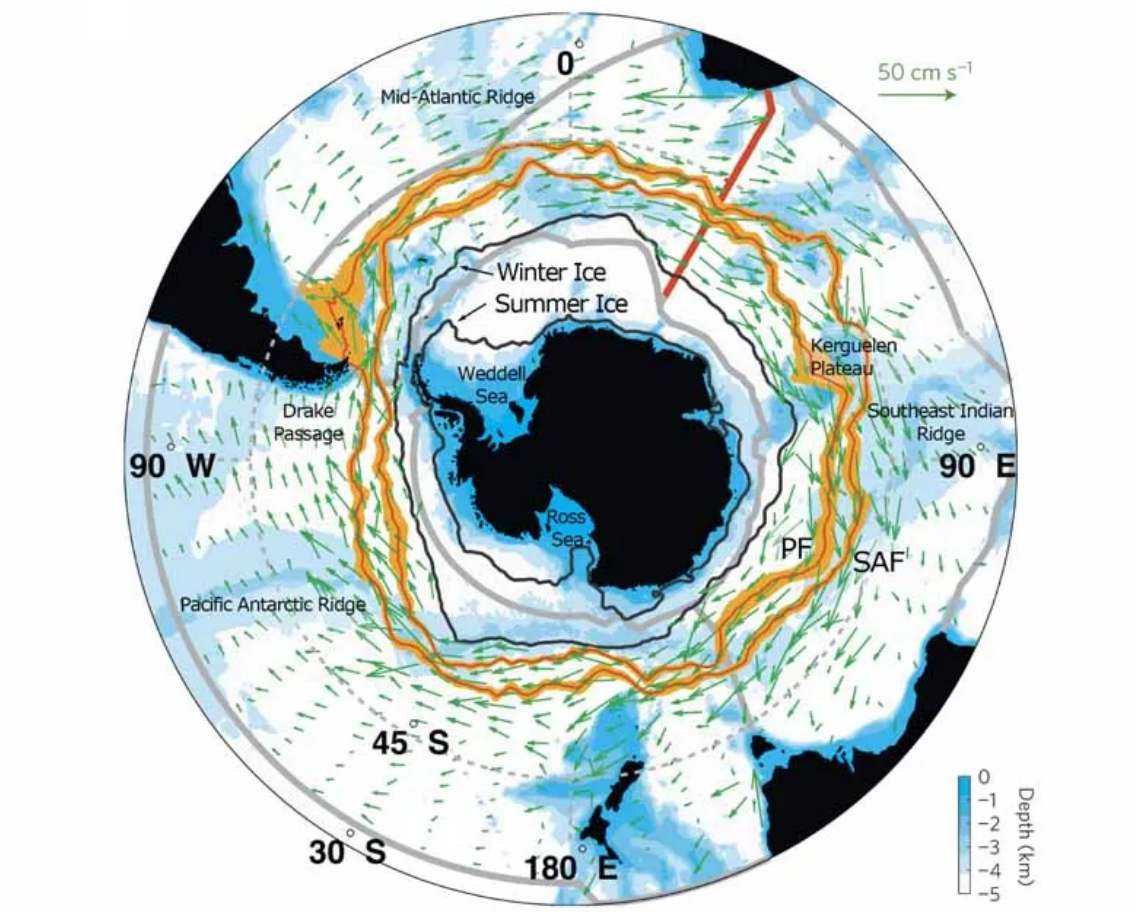

Figure 1.2: Climatological positions of the Antarctic Circumpolar Current (ACC) fronts: the subantarctic fronts (SAF) and polar front (PF) are marked in orange, with the thickness of each line representing the variance in the latitudinal position. Green arrows indicate the observed speed and direction of surface ocean currents (note the scale in the upper right-hand side). Depth of the ocean is shown by color shades. **© Reprinted by permission from Springer Nature: Marshall and Speer (2012)**

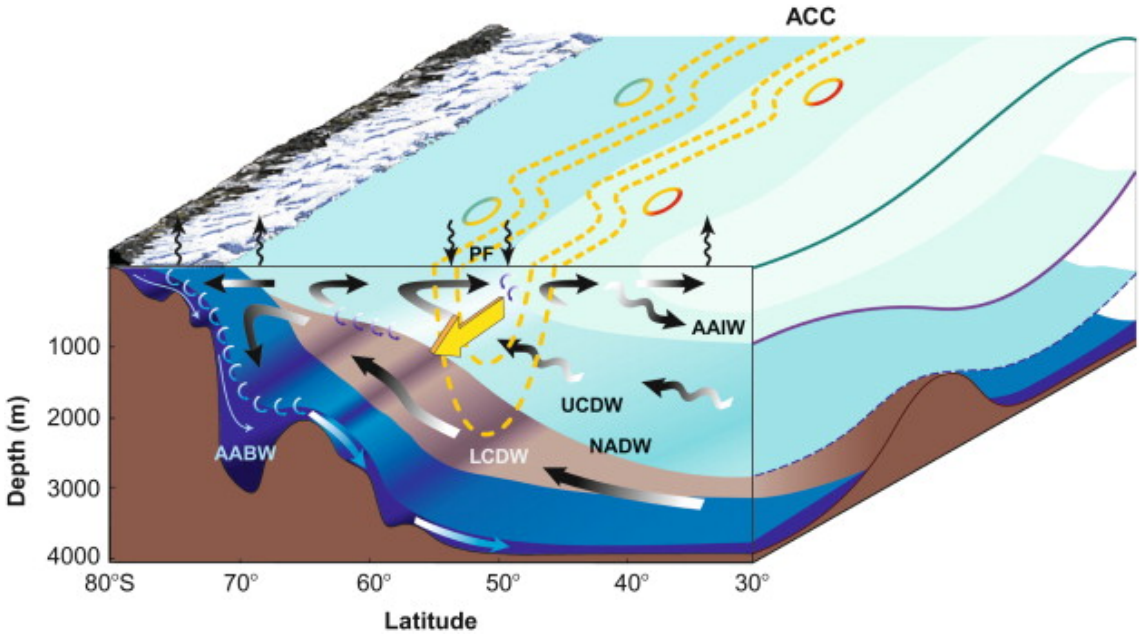

Figure 1.3: Schematic of the ACC (heavy yellow arrow and dashed yellow lines) and the meridional overturning circulation (MOC, dark arrows) in the Southern Ocean. The vertical curly arrows at the sea surface indicate the buoyancy flux. The small light arrows show diapycnal mixing. An upper cell of the MOC is formed primarily by northward Ekman transport beneath the strong westerly winds and southward transport in the Upper Circumpolar Deep Water (UCDW) layer. The lower cell is driven primarily by formation of dense Antarctic Bottom Water (AABW) near the Antarctic continent and inflowing Lower Circumpolar Deep Water (LCDW). From Olbers and Visbeck (2005), adapted from Speer et al. (2000). © **American Meteorological Society. Used with permission.**

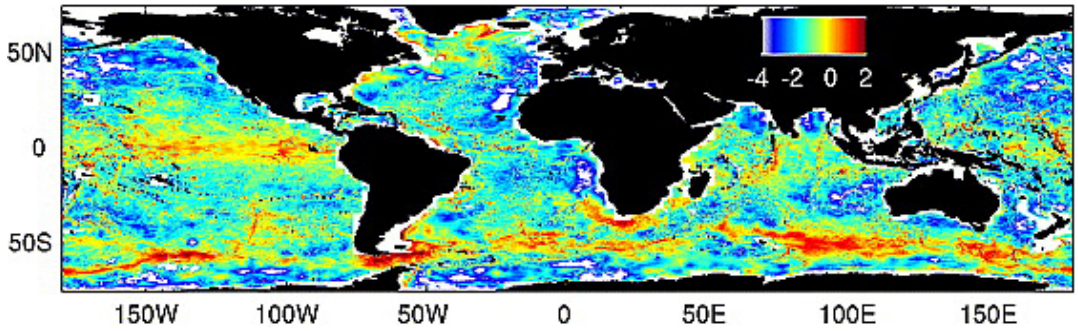

Figure 1.4: Global distribution of the estimated energy flux into internal lee waves, shown in $\log_{10}(\mathrm{mWm}^{-2})$. © **Reprinted by permission from John Wiley and Sons: Nikurashin and Ferrari (2011)**

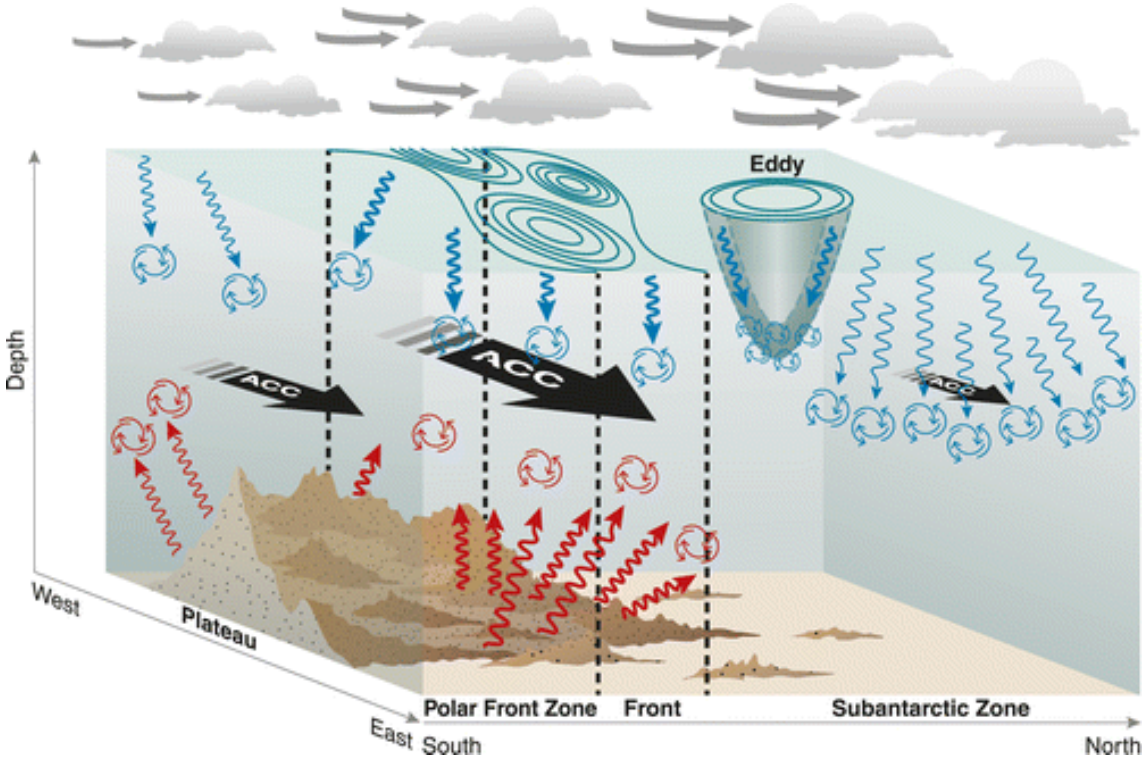

Figure 1.5: Schematic of the spatial distribution of internal waves, mixing, and associated processes north of the Kerguelen Plateau. In the Polar Front zone, mixing intensities are controlled by topographic roughness generating upward-propagating internal waves (red arrows). In the ACC frontal region, strong flows over rough topographic features are associated with enhanced turbulent mixing and with upward-propagating internal lee waves that are advected away from the generation site. In the Subantarctic zone, stronger wind disturbances generate downward-propagating near-inertial waves (blue arrows). Enhanced mixing associated with mesoscale eddy activity is observed north of the frontal region. From Meyer et al. (2015). © **American Meteorological Society. Used with permission.**

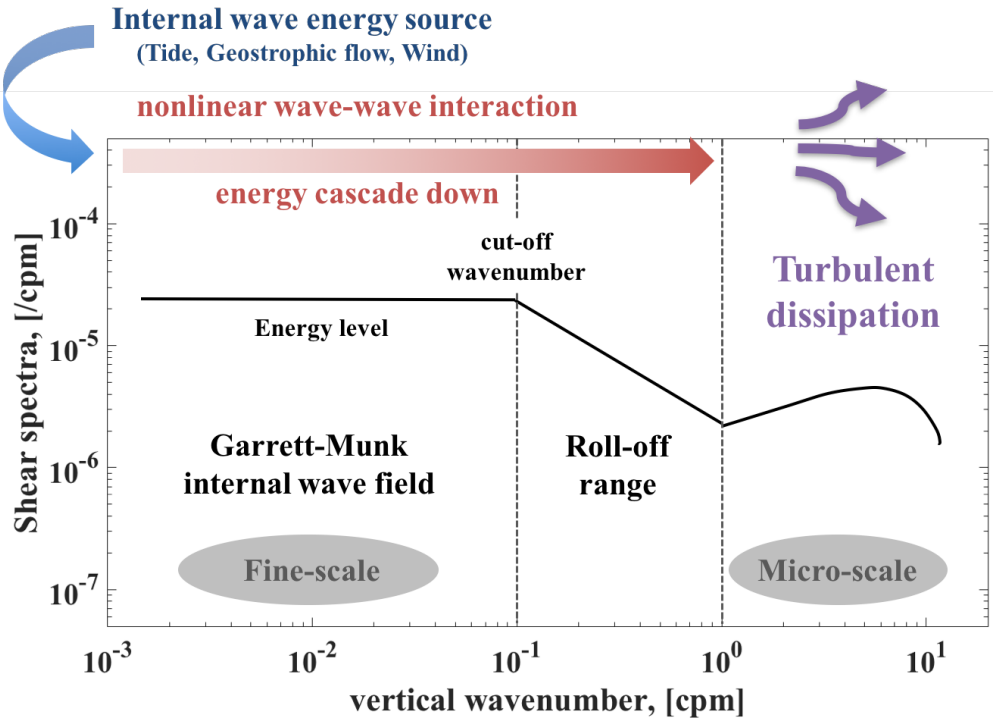

Figure 1.6: Schematic of the energy cascade from finescale internal waves to microscale turbulence superposed on the canonical Garrett-Munk (GM) internal wave spectrum.

Chapter 2

Microstructure Measurements in the Antarctic Circumpolar Current (ACC) Region

2.1 Introduction

The Antarctic Circumpolar Current (ACC) region is considered to be one of the mixing hot spots, where near-inertial waves generated in the upper ocean and internal lee waves generated by the vigorous ACC impinging on rough topographic features break and provide strong turbulent mixing (e.g., Naveira-Garabato et al. 2004). Because of the harsh weather condition and the difficulty of conducting extensive microstructure measurements in the Southern Ocean, the finescale parameterizations (Gregg et al. 2003; Henyey et al. 1986; Polzin et al. 1995; Ijichi and Hibiya 2015) have been used to estimate the distribution of diapycnal mixing (e.g., Naveira-Garabato et al. 2004; Wu et al. 2011). It has been reported, however, that these finescale parameterizations tend to overestimate the actual turbulent dissipation rates in the ACC region (Waterman et al. 2014; Takahashi and Hibiya 2019).

Waterman et al. (2014) analyzed the dataset of the extensive measurements of microstructure and finestructure in the Kerguelen Plateau, and found that the finescale parameterization (Gregg-Henyey-Polzin (GHP) parameterization) robustly and systematically overestimates the turbulent dissipation rates in the bottommost 1500 m at the special locations. These locations were characterized by (1) large predictions of lee wave energy flux (i.e., large near-bottom flow speeds and moderate topographic roughness), (2) low values of shear/strain ratio R_ω indicative of a less near-inertial internal wave field, (3) rotary spectra suggesting a predominance of upward internal wave energy propagation,

(4) enhanced narrowband shear and/or strain variances at vertical wavelengths on the order of 100 m, and (5) elevated near-bottom shear of the background large scale flows. Based on these observed features, Waterman et al. (2014) speculated that wave-mean flow interactions between bottom-generated internal lee waves and the background mean flow shear, which are not considered in the existing finescale parameterization, might be the cause of the observed discrepancy between the actual turbulent dissipation rates and those estimated by the finescale parameterization. We will quantitatively revisit Waterman's hypothesis in Chapter 4.

On the other hand, Takahashi and Hibiya (2019) analyzed the dataset of microstructure and finestructure measurements carried out in the south of Australia, and found that the recently formulated finescale parameterizations (both the GHP and Ijichi-Hibiya (IH) parameterizations) tend to overestimate the actual turbulent dissipation rates at the observation sites located in the ACC jets. The overestimating tendencies of the finescale parameterizations were more correlated with finescale shear and strain variances rather than the large scale vertical shear of the horizontal current speed. In addition, at a station where the finescale parameterizations remarkably overestimated the turbulent dissipation rates, the finescale shear spectrum had a peak at lower vertical wave numbers, which was associated with a nearly monochromatic downward-propagating near-inertial wave packet, so the spectrum was substantially distorted from the typical Garrett-Munk (GM) spectrum. Takahashi and Hibiya (2019) speculated that the overestimates are due to the anisotropy (directivity) of the internal wave field dominated by such a monochromatic wave packet, which is not taken into account in the existing finescale parameterizations, but these results and the speculation were based on much limited number of observations.

In this chapter, we revisit the dataset of the extensive microstructure measurements in the ACC region, which was already analyzed by Waterman et al. (2014), in terms of the distortion of the internal wave field (Takahashi and Hibiya 2019). In addition, we also analyze available datasets of the microstructure and finestructure measurements to

comprehensively examine whether and how the existing finescale parameterizations fail to estimate the actual turbulent dissipation rates in the ACC region.

2.2 Data and analysis

2.2.1 Data

We analyze three datasets of the simultaneous measurements of microstructure and finestructure carried out in the ACC region. The first dataset is from the Southern Ocean Finestructure (SOFine) project conducted in November/December 2008 on the northern flank of the Kerguelen Plateau, where vigorous ACC jets and rough topographic features coexist (red dots in Figure 2.1 and Figure 2.2a). Here the vertical profiles of turbulent dissipation rates, temperature/salinity, and horizontal current speed were measured by free-falling vertical microstructure profilers (VMP-5500), a conductivity-temperature-depth (CTD) profiler, and a lowered acoustic Doppler current profiler (LADCP), respectively. More details of the observations are described in Waterman et al. (2013). Since the number of observation stations is overwhelmingly large, and many of the observation stations were located in the vigorous ACC jets and over the rough topographic features, we will mainly describe the analysis of the SOFine dataset in this dissertation.

The second dataset is from the 19th Kaiyodai Antarctic Research Expedition (KARE19) project conducted in January/February 2016, in which the microstructure measurements were carried out at 10 stations along 110 °E, south of Australia (magenta dots in Figure 2.1). The observation sites extended from the eddying ACC frontal area (e.g., station 2 and 3) to the outside of the ACC region, both the north subtropical zone and the south freezing area (Figure 2.2b), where we deployed a VMP-5500 and a package of the CTD and the LADCP. More details of the observation are described in Takahashi and Hibiya (2019).

The third dataset is from the 21st Kaiyodai Antarctic Research Expedition (KARE21) project conducted in January 2018 at 9 stations (4 stations around 45 °S, 3 stations around

50 °S, and 2 stations around 55 °S) along 110 °E (green dots in Figure 2.1 and Figure 2.2c). Here we used a newly developed instrument "Vertical Microstructure Profiler-eXpendable (VMP-X)" for microstructure measurements. The free-falling VMP-X separates a disposal sensor head when it reaches the sea floor, which makes it possible to observe near-bottom turbulence (Shang et al. 2017). Finescale vertical profiles of density and horizontal current speed were measured by a package of the CTD and the LADCP.

2.2.2 Microstructure analysis

Turbulent dissipation rates were measured using a free-fall VMP-5500 in the SOFine and KARE19 surveys, and a VMP-X in the KARE21 survey, both of which are manufactured by Rockland Scientific International Inc. With reference to Ijichi and Hibiya (2015) and Nagasawa et al. (2007), vertical profiles of microscale velocity shear are divided into consecutive ∼ 10-m-depth bins and vertical wave number shear spectra $\phi(m)$ are calculated using ∼ 1-m-width Hanning windows. In order to eliminate the influence of the instrumental motion, components that are coherent with three-axes (two-axes for VMP-X data) accelerometer signals are subtracted from the raw spectra. The turbulent dissipation rate ε_{micro} at each bin is calculated by integrating $\phi(m)$ from 1 cpm to the highest wave number m_u free from the instrument's vibration noise such that

$$\varepsilon_{micro} = \frac{15}{2}\nu \int_{1\ cpm}^{m_u} \phi(m)\ dm, \tag{2.1}$$

where ν is the kinematic viscosity. If m_u is smaller than the Kolmogorov wave number m_s, the value obtained by integrating the Nasmyth universal spectrum (Nasmyth 1970; Oakey 1982) from m_u to m_s is added to ε_{micro}.

2.2.3 Finestructure analysis

Vertical profiles of finescale temperature and salinity were obtained from CTD measurements. The finescale static stability N^2_{fine} is calculated using the adiabatic leveling method (Bray and Fofonoff 1981),

$$N^2_{fine} = -\frac{g}{\rho_0}\frac{\partial \rho_\theta}{\partial z}, \tag{2.2}$$

where the vertical gradient of the potential density $\partial \rho_\theta / \partial z$ is estimated by a linear regression over a depth bin of 2-m-length after leveling to a midpoint reference pressure, and ρ_0 is the in situ density averaged over the bin. We use the Gibbs-SeaWater Oceanographic Toolbox of TEOS-10 (McDougall and Barker 2011) for calculating the potential density and in situ density. Vertical strain ξ_z is obtained by

$$\xi_z(z) = \frac{N^2_{fine}(z) - N^2(z)}{N^2}, \tag{2.3}$$

where N^2 is the background static stability calculated using the adiabatic leveling method with a 400-m-length bin.

Finescale horizontal velocity was measured mainly using an LADCP, RDI 300-kHz Workhorse, attached to the CTD rosette frame. For the KARE19 and KARE21 surveys, LADCP data are processed using the Lamont-Doherty Earth Observatory processing software (Thurnherr 2011), where 4-m-resolution relative velocity is calculated using "shear method" (Fischer and Visbeck 1993) and 20-m-resolution absolute velocity is calculated using "velocity inversion method" (Visbeck 2002) with bottom-track data and GPS time series as constraints. For the SOFine survey (Waterman et al. 2013), we use the 5-m-resolution "shear method" relative velocity profiles obtained using the software originating from Eric Firing's group at the University of Hawaii and 10-m-resolution absolute velocity profiles obtained using the software from the Lamont-Doherty Earth

Observatory (Visbeck 2002). The finescale parameterizations are applied to the "shear method" profiles.

Only at the stations 1 and 2 in the KARE19 survey, finescale horizontal velocity measured using a Geo-Electronic-Magnetic Current profiler (GEMC) is used, because of the failure of the LADCP measurements[1]. GEMCs measure the horizontal electric field generated by the ocean current crossing the earth's magnetic field. The obtained data are processed following Ijichi and Hibiya (2015), and then horizontal velocity with 5-m-resolution relative to a depth-independent constant is obtained.

2.2.4 Application of finescale parameterizations

In this study, we compare the turbulent dissipation rates ε measured using VMPs and those estimated by the two kinds of existing finescale parameterizations, the Gregg-Henyey-Polzin (GHP) parameterization (Gregg et al. 2003; Henyey et al. 1986; Polzin et al. 1995) and Ijichi-Hibiya (IH) parameterization (Ijichi and Hibiya 2015).

Both the GHP and IH parameterizations estimate ε from the finescale shear and strain spectral levels. The GHP parameterization was formulated so as to improve the accuracy of the previous finescale parameterizations (Gregg 1989; Wijesekera et al. 1993) by introducing a parameter, shear/strain ratio R_ω, to consider the distortion of the frequency spectrum of the internal wave energy from the Garrett-Munk (GM) model (Garrett and Munk 1975; Cairns and Williams 1976). Recently, Ijichi and Hibiya (2015) improved the frequency correction term in the GHP parameterization and showed their IH parameterization can predict ε more accurately than the GHP parameterization in the Izu-Ogasawara Ridge where the internal wave energy spectra are significantly biased to near-inertial frequencies.

Since the weak nonlinear wave-wave interaction theory adopted in the finescale pa-

[1] At the station 3 of the KARE19, the rudders and the rudder ring of the GEMC, which were attached so as to rotate the instrument, got damaged. It's unclear whether this is the cause or not, but since the GEMC data were quite inconsistent with the LADCP data after the station 3, we gave up using it for analysis.

rameterizations becomes no longer applicable in the vicinity of the boundary, surface 400 m, bottom 400 m, and profiles obtained on the continental shelf (station 8 of the KARE19 survey) are excluded from the analysis. Vertical profiles of the finescale horizontal velocity and density are divided into half-overlapping 400-m-length bins. Vertical wave number spectra of shear and strain are calculated after subtracting a linear trend. Furthermore, we apply some corrections to the finescale shear spectra obtained from the LADCP shear method (Thurnherr 2012). In order to minimize possible errors, shear and strain spectra are averaged over three adjacent bins. These spectra are integrated from the minimum vertical wave number m_{low} (= 0.0025 cpm, the corresponding wavelength λ_z = 400 m) to the cut-off wave number m_c to obtain the (buoyancy-normalized) shear variance $\left\langle U_z^2/N^2 \right\rangle$ and strain variance $\left\langle \xi_z^2 \right\rangle$.

The cut-off wave number m_c is set to be the smallest one out of the following three criteria.

1. The wave number at which the power spectrum density of the horizontal velocity fluctuation becomes less than the instrumental noise level.

2. The wave number at which the shear spectrum starts to roll off. The second criterion is set based on the empirical shear spectrum model (Gargett et al. 1981; Munk 1981), in which the spectrum is flat at lower vertical wave numbers, then falls as m^{-1} to the buoyancy wave number $k_b = \left(N^3/\varepsilon\right)^{1/2}$, and the transition wave number m_c^{Ri} between two regimes is determined from the following Richardson-like function such as (Gregg et al. 2003),

$$\int_0^{m_c^{Ri}} \Phi_{Fr}(m)\, dm = \int_0^{m_c^{GM}} \Phi_{Fr}^{GM}(m)\, dm = 0.66. \tag{2.4}$$

Here $\Phi_{Fr}(m)$ is the buoyancy-normalized shear spectrum (the Froude spectrum), $\Phi_{Fr}^{GM}(m)$ and m_c^{GM} = 0.1 cpm are the Froude spectrum and the roll-off wave number of the GM spectrum model. Hereinafter the cut-off wave number determined from

this criteria m_c^{Ri} is referred to as the "Richardson number-based (*Ri*-based) cut-off wave number".

3. m_c^{LAD} = 0.015 cpm (λ_z = 67 m). The third criterion is set based on the fact that m = 0.02 cpm (λ_z = 50 m) is the maximum vertical wave number below which LADCP shear spectra are coherent with expendable current profiler (XCP) shear spectra (Polzin et al. 2002; Thurnherr 2012). It is well known that the LADCP shear spectrum is dominated by noise at higher wave numbers. Hereinafter, the cut-off wave number determined from this criteria m_c^{LAD} is referred to as the "LADCP-based cut-off wave number".

For the most of the spectra analyzed in this study, the cut-off wave number is determined from the third criterion, so that the wavelength band λ_z = 67 – 400 m is used for the calculation of the finescale parameterizations. It should be noted that the previous studies also used the similar wavelength band such as λ_z = 130 – 320 m (Waterman et al. 2013), λ_z = 60 – 180 m (Sheen et al. 2013), and λ_z = 50 – 256 m (Kunze 2017).

Obtained shear and strain variances are incorporated into the following equations of the GHP and IH parameterizations,

$$\varepsilon_{GHP} = \varepsilon_0 \, (N/N_0)^2 \left(\left\langle U_z^2/N^2 \right\rangle / \left\langle U_z^2/N^2 \right\rangle_{GM} \right)^2 h_{GHP}(R_\omega, f, N), \tag{2.5}$$

$$\varepsilon_{IH} = \varepsilon_0 \, (N/N_0)^2 \left(\left\langle U_z^2/N^2 \right\rangle / \left\langle U_z^2/N^2 \right\rangle_{GM} \right)^2 h_{IH}(R_\omega, f, N), \tag{2.6}$$

where ε_0 and $N_0 = 5.2 \times 10^{-3}$ s^{-1} are the constant coefficients, and f is the Coriolis frequency. While we use the empirical constant coefficient $\varepsilon_0 = 6.3 \times 10^{-10}$ W/kg (Gregg et al. 2003) for the SOFine and KARE19 datasets, the doubled value $\varepsilon_0 = 1.26 \times 10^{-9}$ W/kg is used for the KARE21 dataset. This is because our several simultaneous measurements using a VMP-5500 and VMP-X in the Indonesian Archipelago showed that turbulent dissipation rates measured by the VMP-X were, on average, twice as large as those measured by the VMP-5500 (Figure 2.3).

In the finescale parameterizations (2.5) and (2.6), turbulent dissipation rates are primarily estimated from the shear spectral level, in other words, the shear variance normalized by the corresponding GM spectral level. The shear/strain ratio,

$$R_\omega = \frac{\left\langle U_z^2/N^2 \right\rangle}{\left\langle \xi_z^2 \right\rangle}, \tag{2.7}$$

is a parameter indicating the bulk frequency content of the internal wave field. Larger R_ω values ($R_\omega \gg 3$) imply the dominance of near-inertial waves, while smaller R_ω values ($R_\omega < 3$) can be attributed to the presence of more high frequency internal waves. The frequency dependent terms in the GHP and IH parameterizations are,

$$h_{GHP}(R_\omega, f, N) = \frac{1 + 1/R_\omega}{4/3} \sqrt{\frac{2}{R_\omega - 1}} \frac{f \cosh^{-1}(N/f)}{f_0 \cosh^{-1}(N_0/f_0)}, \tag{2.8}$$

$$h_{IH}(R_\omega, f, N) = \begin{cases} \frac{1+1/R_\omega}{4/3} \frac{L_1}{L_0} R_\omega^{-L_2} & (R_\omega < 9), \\ \frac{1+1/R_\omega}{4/3} \frac{1}{L_0} \sqrt{\frac{2}{R_\omega - 1}} & (R_\omega > 9), \end{cases} \tag{2.9}$$

$$\begin{aligned} L_0 &= 2\pi^{-1} \cosh^{-1}(N_0/f_0), \\ \mu_{GM} &= 2\pi^{-1} \cosh^{-1}(N/f), \\ L_1 &= 2\mu_{GM}^2, \\ L_2 &= \log_3(2\mu_{GM}). \end{aligned}$$

From the finescale shear and strain spectra, we can obtain three parameters that characterize the background internal wave field. The first parameter is the shear/strain ratio R_ω (2.7) already explained above. The second parameter is the internal wave energy

level,

$$E_{IW} = \frac{\left\langle U_z^2/N^2 \right\rangle + \left\langle \xi_z^2 \right\rangle}{\left\langle U_z^2/N^2 \right\rangle_{GM} + \left\langle \xi_z^2 \right\rangle_{GM}}, \tag{2.10}$$

which indicates how large the internal wave energy compared to the GM spectrum model.

The third parameter is the rotary coefficient C_R, which is an indicator of the vertical propagation direction of the internal wave energy. To calculate the rotary coefficient, the vertical profile of the horizontal velocity vector $(u(z), v(z))$ is decomposed into spectral components that rotate clockwise $\Phi_{CW}(m)$ and counterclockwise $\Phi_{CCW}(m)$ in the vertical direction (Gonella 1972; Leaman and Sanford 1975). If we assume that each Fourier component of the horizontal velocity spectrum with vertical wave number m corresponds to single internal wave packet, its vertical propagation direction can be estimated by using the fact that an internal wave with downward (upward) group velocity satisfies $\Phi_{CCW}(m) > \Phi_{CW}(m)$ ($\Phi_{CCW}(m) < \Phi_{CW}(m)$) in the Southern Hemisphere. The rotary coefficient is defined as,

$$C_R = \frac{\left\langle U_z^2/N^2 \right\rangle_{\Phi_{CCW}>\Phi_{CW}} - \left\langle U_z^2/N^2 \right\rangle_{\Phi_{CCW}<\Phi_{CW}}}{\left\langle U_z^2/N^2 \right\rangle_{total}}, \tag{2.11}$$

where in the numerator the shear spectrum is integrated for the wave number satisfying $\Phi_{CCW}(m) > \Phi_{CW}(m)$ or $\Phi_{CCW}(m) < \Phi_{CW}(m)$, respectively. The values of the rotary coefficient $C_R > 0$ ($C_R < 0$) imply the dominance of the downward-propagating (upward-propagating) internal wave energy. It should be noted, however, that this analysis is reliable only when the frequency of the internal wave packet is near-inertial. As the frequency of the internal wave packet approaches the buoyancy frequency, the ratio Φ_{CCW}/Φ_{CW} asymptotically approaches 1 regardless of the vertical propagation direction, so the estimate is no longer robust. See Appendix 2.A. for detailed explanation of the definition and derivation of C_R.

2.3 Results

本節については、5 年以内に雑誌等で刊行予定のため、非公開。

2.4 Concluding remarks

本節については、5 年以内に雑誌等で刊行予定のため、非公開。

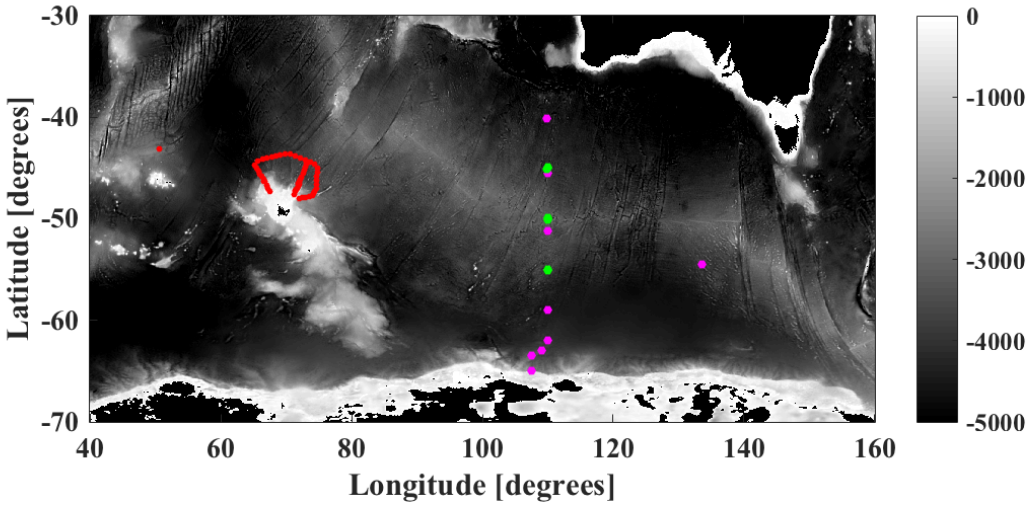

Figure 2.1: Locations of the observation stations of the SOFine (red), KARE19 (magenta), and KARE21 (green) surveys. Depth [m] is shown by shading.

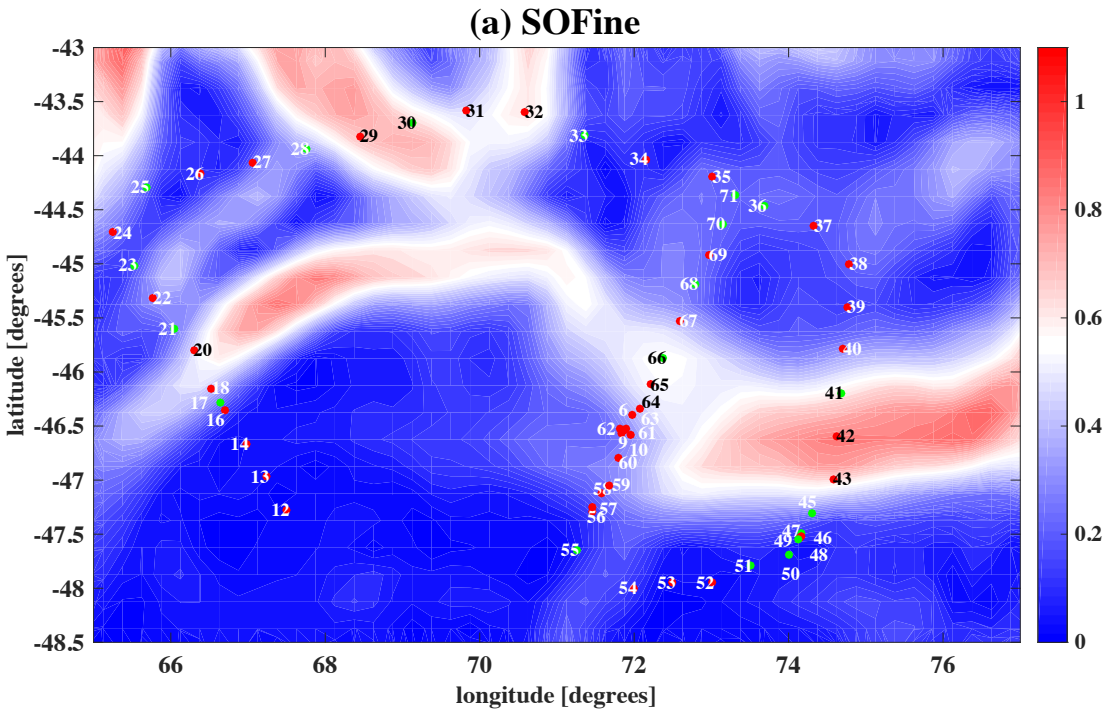

Figure 2.2: Surface geostrophic current speed [m/s] during the survey of (a) SOFine, (b) KARE19, and (c) KARE21. Data are obtained from Archiving, Validation, and Interpretation of Satellite Oceanographic data (AVISO). Locations of the observation stations are superposed on the map with station numbers. For the (a) SOFine survey, red dots indicate the observation stations at which both microstructure and finestructure measurements were carried out, while green dots indicate the observation stations at which only finestructure measurements were carried out. Note that the station 4 of the SOFine survey located at (50.6°E, 43.2°S).

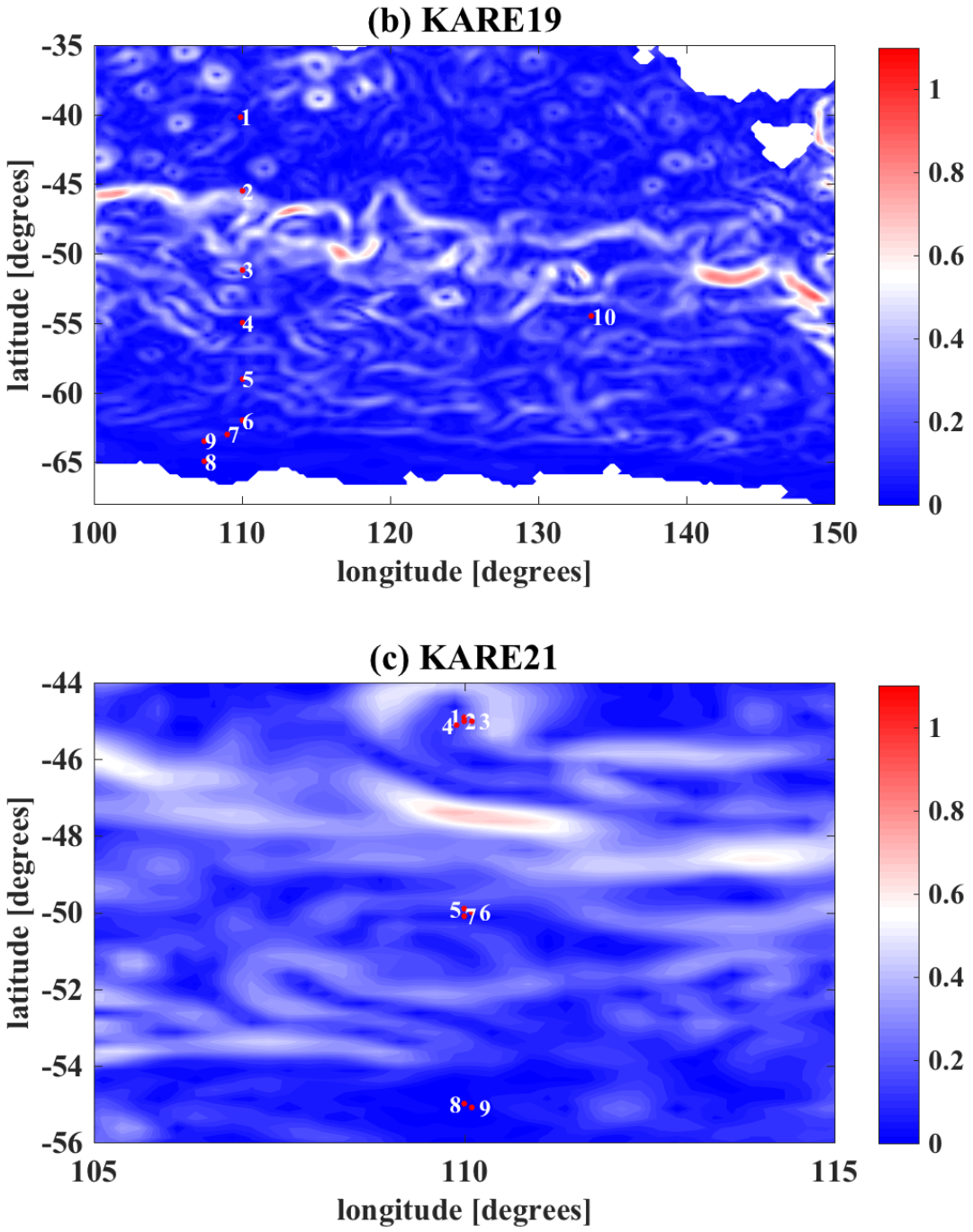

Figure 2.2: Surface geostrophic current speed [m/s] during the survey of (a) SOFine, (b) KARE19, and (c) KARE21. Data are obtained from Archiving, Validation, and Interpretation of Satellite Oceanographic data (AVISO). Locations of the observation stations are superposed on the map with station numbers.

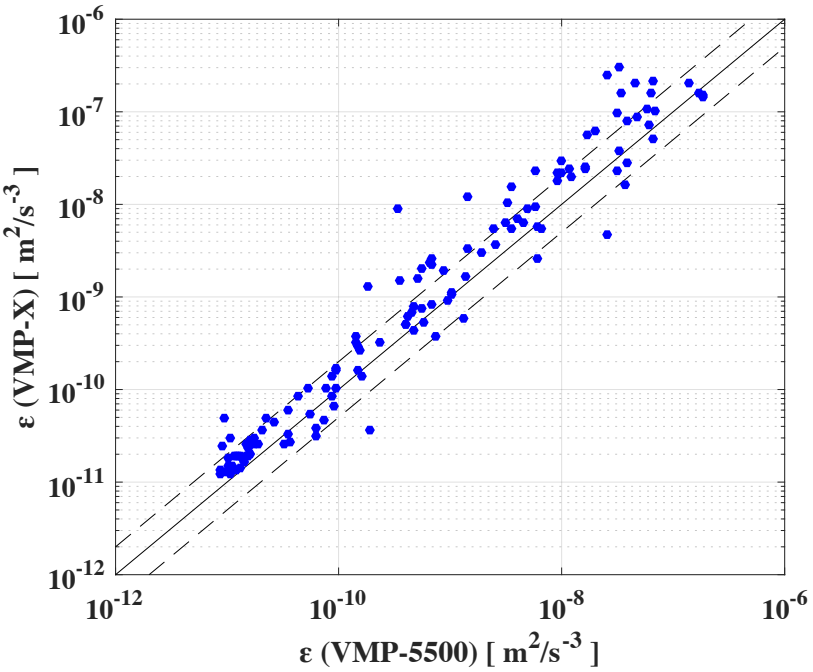

Figure 2.3: Relationship between the turbulent dissipation rates ε obtained by a VMP-5500 and those obtained by a VMP-X. Both profilers were simultaneously deployed in the Indonesian Archipelago. Solid line is drawn such that ε (VMP-5500) and ε (VMP-X) are the same value, and dashed lines are drawn such that the difference is a factor of two.

Appendix 2.A Derivation and interpretation of the rotary coefficient

In this appendix, the derivation and definition of the rotary coefficient C_R are summarized. When we calculate the frequency spectrum of horizontal current speed, it can be treated as a vector time series of two orthogonal components, instead of a scalar time series. Gonella (1972) extended this idea and proposed a method to separate the velocity component rotating clockwise and counterclockwise with time. Then, Leaman and Sanford (1975) applied this technique to the vertical profile of the horizontal current speed, which was used to estimate the vertical propagating direction of the internal wave energy.

2.A.1 Derivation of the rotary component spectra

The symbol w is defined as the complex quantity,

$$w = u + iv, \tag{2.12}$$

where (u, v) are two orthogonal components of horizontal velocity. The Fourier components of the (u, v) with a vertical wave number $m > 0$ are,

$$u_m(z) = a_{1m}\cos(mz) + b_{1m}\sin(mz), \tag{2.13}$$

$$v_m(z) = a_{2m}\cos(mz) + b_{2m}\sin(mz), \tag{2.14}$$

with the Fourier coefficients a and b. Here w_m can be decomposed into two velocity components rotating in opposite directions,

$$w_m = u_m + iv_m = u_{+m}\mathrm{e}^{imz} + u_{-m}\mathrm{e}^{-imz}. \tag{2.15}$$

If z is taken so that the downward direction is positive, u_{+m} is the counterclockwise (CCW) rotary component and u_{-m} is the clockwise (CW) rotary component with depth. Thus,

removing the subscript m,

$$u_+ = \frac{1}{2}\{(a_1 + b_2) + i(a_2 - b_1)\}, \tag{2.16}$$

$$u_- = \frac{1}{2}\{(a_1 - b_2) + i(a_2 + b_1)\}. \tag{2.17}$$

The power spectra of the CCW and CW rotary component velocity are,

$$\Phi_{CCW} = 2u_+^* u_+, \tag{2.18}$$

$$\Phi_{CW} = 2u_-^* u_-, \tag{2.19}$$

where * indicates the complex conjugate. The total power spectrum is,

$$\Phi_{total} = \Phi_{CCW} + \Phi_{CW}. \tag{2.20}$$

Using the auto-spectrum of the horizontal current speed P_{uu}, P_{vv}, and the quadrature spectrum Q_{uv},

$$P_{uu} = a_1^2 + b_1^2, \tag{2.21}$$

$$P_{vv} = a_2^2 + b_2^2, \tag{2.22}$$

$$Q_{uv} = a_1 b_2 - a_2 b_1, \tag{2.23}$$

the CCW and CW rotary component spectra are expressed as

$$\Phi_{CCW} = \frac{1}{2}\left(P_{uu} + P_{vv} + 2Q_{uv}\right), \tag{2.24}$$

$$\Phi_{CW} = \frac{1}{2}\left(P_{uu} + P_{vv} - 2Q_{uv}\right). \tag{2.25}$$

2.A.2 Interpretation of the rotary coefficient

Linear internal waves have temporal-spatial structures[2] $\propto e^{i(kx+mz-\sigma t)}$ with zonal wave number k, vertical wave number[3] m, and intrinsic frequency $\sigma > 0$. Horizontal velocity of the linear internal wave is expressed as,

$$u = \hat{u}\cos(kx + mz - \sigma t), \tag{2.26}$$

$$v = \frac{f}{\sigma}\hat{u}\sin(kx + mz - \sigma t), \tag{2.27}$$

which has an elliptical orbit with a major radius $|\hat{u}|$ and minor radius $|f\hat{u}/\sigma|$. Hereinafter, the situation in the Southern Hemisphere ($f < 0$) is considered.

For inertial waves ($\sigma = |f|$), the vertical variation of the horizontal velocity (x and t are set to be constant) is,

$$(u, v) = \hat{u}(\cos mz, -\sin mz), \tag{2.28}$$

$$= \hat{u}\mathrm{e}^{-imz}, \tag{2.29}$$

namely, the velocity vector turns round clockwise (counterclockwise) with depth if $m > 0$ ($m < 0$).

For near-inertial waves with frequency $\sigma \sim |f|$, the vertical variation of the horizontal velocity vector has an elliptical but nearly circular orbit. From equations (2.24) and (2.25), the ratio of the CCW rotary component to the CW rotary component is,

$$\Phi_{CCW}/\Phi_{CW} = \begin{cases} \left(\frac{\sigma-|f|}{\sigma+|f|}\right)^2 & (m > 0), \\ \left(\frac{\sigma+|f|}{\sigma-|f|}\right)^2 & (m < 0), \end{cases} \tag{2.30}$$

indicating that the CW (CCW) rotary component is dominant for the near-inertial waves

[2]For simplicity, the meridional wave number l is ignored here.
[3]Hereinafter, m can take both positive and negative values.

with vertical wave number $m > 0$ ($m < 0$). The vertical phase velocity C_{pz} and the vertical group velocity C_{gz} are,

$$C_{pz} = \frac{\sigma}{m}, \tag{2.31}$$

$$C_{gz} = -\frac{(\sigma^2 - f^2)(N^2 - \sigma^2)}{\sigma m(N^2 - f^2)}. \tag{2.32}$$

These relationships indicate that the near-inertial waves with $m > 0$ ($m < 0$) roughly rotate CW (CCW) and their energy propagates upward (downward)[4].

For super-inertial waves ($\sigma \gg |f|$), the vertical variation of the horizontal velocity has a straight line orbit. Equation (2.30) indicates that $\Phi_{CCW}/\Phi_{CW} \to 1$ for the super-inertial waves with $\sigma \gg |f|$, regardless of the sign of m. In other words, for the super-inertial waves, the vertical propagation direction cannot be detected robustly from the rotary component spectral analysis.

2.A.3 Definition of the rotary coefficient

Applying the method explained in section 2.A.1 to the buoyancy-normalized shear spectrum (the Froude spectrum), we derive the CCW and CW rotary components of the Froude spectrum, Φ^{Fr}_{CCW} and Φ^{Fr}_{CW}. As already explained in section 2.A.2 (see equation (2.30)), internal waves with $m > 0$ ($m < 0$) have more CW (CCW) rotary component energy rather than CCW (CW) rotary component energy. The rotary coefficient C_R is defined as,

$$C_R = \frac{\left\langle U_z^2/N^2 \right\rangle_{\Phi_{CCW} > \Phi_{CW}} - \left\langle U_z^2/N^2 \right\rangle_{\Phi_{CCW} < \Phi_{CW}}}{\left\langle U_z^2/N^2 \right\rangle_{total}}, \tag{2.33}$$

where the component of the numerator indicates, for example, the integrates such as

$$\left\langle U_z^2/N^2 \right\rangle_{\Phi_{CCW} > \Phi_{CW}} = \int_{C_1} \Phi^{Fr}(m)\, dm, \tag{2.34}$$

[4]Note that z is taken so that the downward direction is positive.

with an integration path $C_1 : m_{low} < m < m_c$ satisfying $\Phi^{Fr}_{CCW}(m) > \Phi^{Fr}_{CW}(m)$. Since the denominator of (2.33) satisfies the following equation,

$$\left\langle U_z^2/N^2 \right\rangle_{total} = \left\langle U_z^2/N^2 \right\rangle_{\Phi_{CCW}>\Phi_{CW}} + \left\langle U_z^2/N^2 \right\rangle_{\Phi_{CCW}<\Phi_{CW}}, \tag{2.35}$$

the rotary coefficient ranges $-1 \leq C_R \leq 1$. It is suggested that the downward-propagating (upward-propagating) near-inertial wave energy is dominant if $C_R > 0$ ($C_R < 0$).

Note that the polarization ratio $R_{CCW/CW}$ as an indicator of the vertical propagation direction of the internal wave energy,

$$R_{CCW/CW} = \frac{\int_{m_{low}}^{m_c} \Phi^{Fr}_{CCW}(m)\, dm}{\int_{m_{low}}^{m_c} \Phi^{Fr}_{CW}(m)\, dm}, \tag{2.36}$$

used in many of the oceanographic literatures (e.g., Waterman et al. 2013, 2014; Sheen et al. 2013) is misleading (Dr. Kaoru Sato, personal communication 2019).

Chapter 3

Eikonal Calculations I : Influence of the Distortion of the Internal Wave Spectrum

3.1 Introduction

In Chapter 2, we have shown that the existing finescale parameterizations (Gregg et al. 2003; Henyey et al. 1986; Polzin et al. 1995; Ijichi and Hibiya 2015) tend to overestimate the actual turbulent dissipation rates in the Antarctic Circumpolar Current (ACC) region where the eddying geostrophic flows coexist with the internal wave field. These overestimates are well correlated with the internal wave parameters, such as the shear/strain ratio R_ω and the internal wave energy level E_{IW} rather than the large scale background (mean flow) shear. The discrepancy between the turbulent dissipation rates directly measured and those estimated becomes more evident as E_{IW} increases and R_ω decreases.

In addition, at the locations where the finescale parameterizations significantly overestimate the turbulent dissipation rates, the finescale shear and strain spectra have humps at low vertical wave numbers. With the assumption that the vertical wave number spectra of the finescale shear and strain are flat like the Garrett-Munk (GM) spectrum (Garrett and Munk 1972, 1975; Cairns and Williams 1976; Munk 1981), the finescale parameterizations estimate the turbulent dissipation rates from the shear and strain spectral levels in the lower vertical wave number band. This is because the finescale shear spectrum, especially obtained by a lowered acoustic Doppler current profiler (LADCP), is usually contaminated by noise at higher vertical wave numbers.

On the basis of the above observed clues, it is reasonable to relate the discrepancy between the measured and estimated turbulent dissipation rates to the distortion of the finescale internal wave energy spectrum. However, whether and how the finescale parameterizations overestimate the turbulent dissipation rates for the internal wave spectrum with a "hump" are still unclear and should be investigated quantitatively.

In this chapter, we carry out several numerical experiments called "eikonal calculations" to quantitatively examine the energy cascade within the internal wave spectrum with a low vertical wave number hump.

3.2 Eikonal calculations

本節については、5 年以内に雑誌等で刊行予定のため、非公開。

3.3 Standard experiment

本節については、5 年以内に雑誌等で刊行予定のため、非公開。

3.4 Hump experiments

本節については、5 年以内に雑誌等で刊行予定のため、非公開。

3.5 Conclusions and discussions

本節については、5 年以内に雑誌等で刊行予定のため、非公開。

Appendix 3.A Background velocity field of the Garrett-Munk (GM) spectrum

本節については、5 年以内に雑誌等で刊行予定のため、非公開。

Appendix 3.B Background velocity field for the hump experiments

本節については、5 年以内に雑誌等で刊行予定のため、非公開。

Chapter 4

Eikonal Calculations II : Influence of the Large Scale Mean Flow Shear

4.1 Introduction

In the previous chapters, we have shown that the vertical wave number spectra of the finescale shear and strain are distorted from the flat-shaped Garrett-Munk (GM) spectrum (Garrett and Munk 1972, 1975; Cairns and Williams 1976; Munk 1981) in the Antarctic Circumpolar Current (ACC) region (Chapter 2), and the existing finescale parameterization (Ijichi and Hibiya 2015) overestimates the actual turbulent dissipation rates for such internal wave field (Chapter 3).

On the other hand, Waterman et al. (2014) pointed out from the observation results that the locations at which the finescale parameterization overestimated the turbulent dissipation rates were associated with the large background flow shear $\overline{U_z}$[1] (Figure 4.1). According to Waterman et al. (2014), the importance of wave-mean flow interactions relative to nonlinear wave-wave interactions in the spectral energy cascade can be evaluated by the magnitude of the Froude number $Fr = \overline{U_z}/N$ with the buoyancy frequency N.

In addition, Waterman et al. (2014) pointed out that all of the locations where the finescale parameterization overestimated the turbulent dissipation rates also exhibited an atypical background shear in which the flow magnitude decreased with height above bottom, and they speculated that such background flows would force the upward-propagating

[1]While $\overline{U_z}$ was estimated from the vertical profile of the horizontal current speed smoothed by a sliding polynomial fit over a vertical scale of 300 m in Waterman et al. (2014), we believe it would be a similar value to the "mean flow shear" estimated from the 800-m linear-fit in Chapter 2.

waves towards the internal wave critical layer situation. They expected, in such a scenario, that wave-mean flow interactions could suppress the internal wave breaking, and it would explain the discrepancy between the directly-measured turbulent dissipation rates and those estimated by the finescale parameterization. Quite recently, Kunze and Lien (2019) analytically formulated this hypothesis and quantified the impact of wave-mean flow interactions by giving an idealized horizontal wave number spectrum for topographic height $S[h](k) \propto k^{-n}$, where $n = -2.5 \pm 0.3$ is the topographic height spectral slope characteristic for the Southern Ocean (Nikurashin and Ferrari 2010; Waterman et al. 2014). Details of the speculation by Waterman et al. (2014) will be described in the next section.

Waterman's hypothesis, however, has not yet been quantitatively verified. In this chapter, we carry out eikonal calculations to quantitatively examine whether the finescale parameterization can overestimate the turbulent dissipation rates due to the wave-mean flow interactions, for the realistic situation where the observed magnitude of the background flow shear coexists with the internal wave field.

4.2 Hypothesis in Waterman et al. (2014)

Waterman et al. (2014) and Kunze and Lien (2019)[2] attempted to explain why the finescale parameterization overestimates turbulent dissipation rates in the ACC region using a simple conceptual model (see Figure 4.2) consists of a monochromatic lee wave packet and a background mean flow shear with zonal velocity $U_{mean} > 0$ and its vertical shear $dU_{mean}/dz < 0$.

The mean flow with bottom current speed $U_{bot} > 0$ impinges on the bottom topographic features with zonal wave number k and creates an internal lee wave packet with intrinsic frequency $\sigma = -U_{bot}k > 0$, where we define the frequency σ as a positive value, and therefore $k < 0$. Since the bottom-generated lee wave propagates upward, its vertical wave

[2]Kunze and Lien (2019) considered the multichromatic lee wave generation using the topographic height spectrum, but assumed that each lee wave packet is Doppler shifted only by the background mean flow shear and is not affected by other lee wave packets.

number,

$$m = k\sqrt{\frac{N^2 - k^2U_{bot}^2}{k^2U_{bot}^2 - f^2}} < 0, \tag{4.1}$$

with f the Coriolis frequency is a negative value, and it can be approximated such that $m \sim -N/U_{bot}$ for $f \ll \sigma = |U_{bot}k| \ll N$.

The generated lee wave packet propagates upward while increasing the magnitude of its vertical wave number $|m|$ and decreasing its intrinsic frequency σ according to the following eikonal equations,

$$\begin{aligned} \mathbf{k_H} &= const., \\ \frac{dm}{dt} &= -k\frac{dU_{mean}}{dz}, \end{aligned}$$

where $\mathbf{k_H} = (k, l)$ is the lee wave's horizontal wave number vector, and the dispersion relation of the internal waves,

$$\sigma = \sqrt{\frac{N^2(k^2 + l^2) + f^2m^2}{k^2 + l^2 + m^2}}. \tag{4.2}$$

It should be noted here that lee wave's horizontal wave number $\mathbf{k_H}$ does not change because there only exist a monochromatic lee wave packet and a zonal mean flow U_{mean} with vertical shear. Considering the conservation of wave action $A = E/\sigma$ (Bretherton and Garrett 1968), energy of a lee wave packet when it breaks E^{fin} is smaller than that when it is generated at the bottom E^{init}. The difference $\Delta E = E^{init} - E^{fin}$ is the energy transferred to the background from the wave packet. Waterman et al. (2014) and Kunze and Lien (2019) considered that the discrepancy between the actual turbulent dissipation rates and those estimated by the finescale parameterization is due to this ΔE caused by wave-mean flow interaction between the lee wave packet and the mesoscale eddies associated with the ACC.

本部分については、5 年以内に雑誌等で刊行予定のため、非公開。

4.3 Lee wave packet experiments

本節については、5 年以内に雑誌等で刊行予定のため、非公開。

4.4 Spectrum experiments

本節については、5 年以内に雑誌等で刊行予定のため、非公開。

4.5 Concluding remarks

本節については、5 年以内に雑誌等で刊行予定のため、非公開。

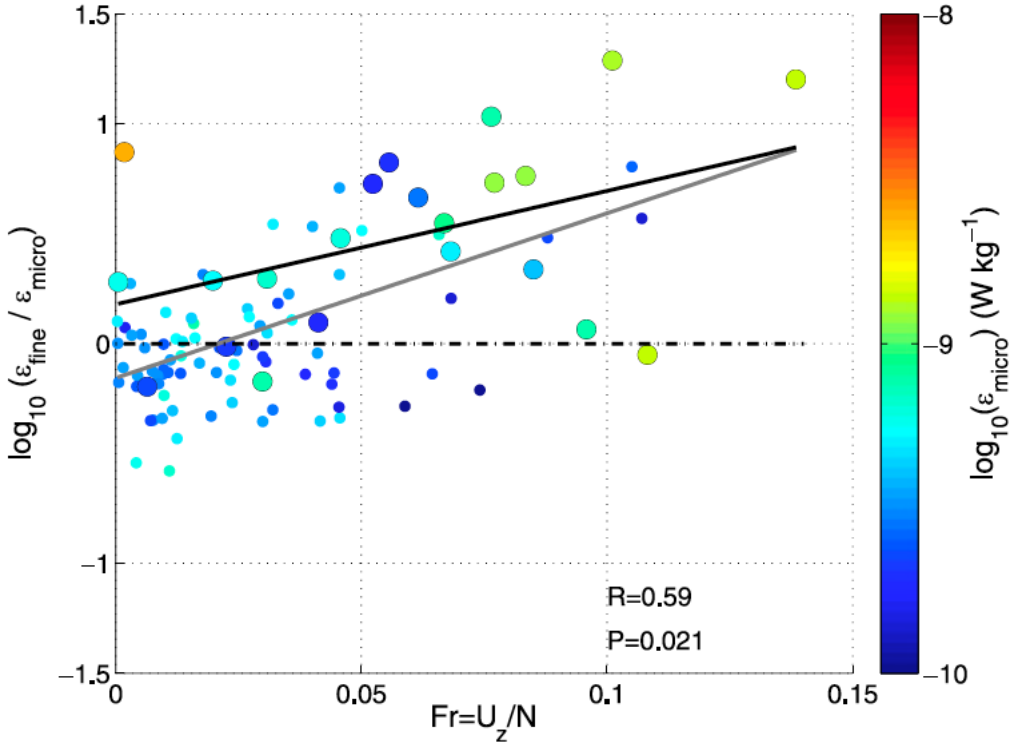

Figure 4.1: Relationship between the Froude number $Fr = \overline{U_z}/N$ and the overestimates of the turbulent dissipation rates by the finescale parameterization near the bottom (specifically height above bottom < 1000 m). Points are colored by the value of ε_{micro}. Lines show the result of a linear regression of the ratio $\varepsilon_{fine}/\varepsilon_{micro}$ on the Froude number for the full dataset (black) and the selected eight stations only (gray). Regression statistics are displayed in the lower right-hand corner for the full dataset. Adapted from from Waterman et al. (2014). © **American Meteorological Society. Used with permission.**

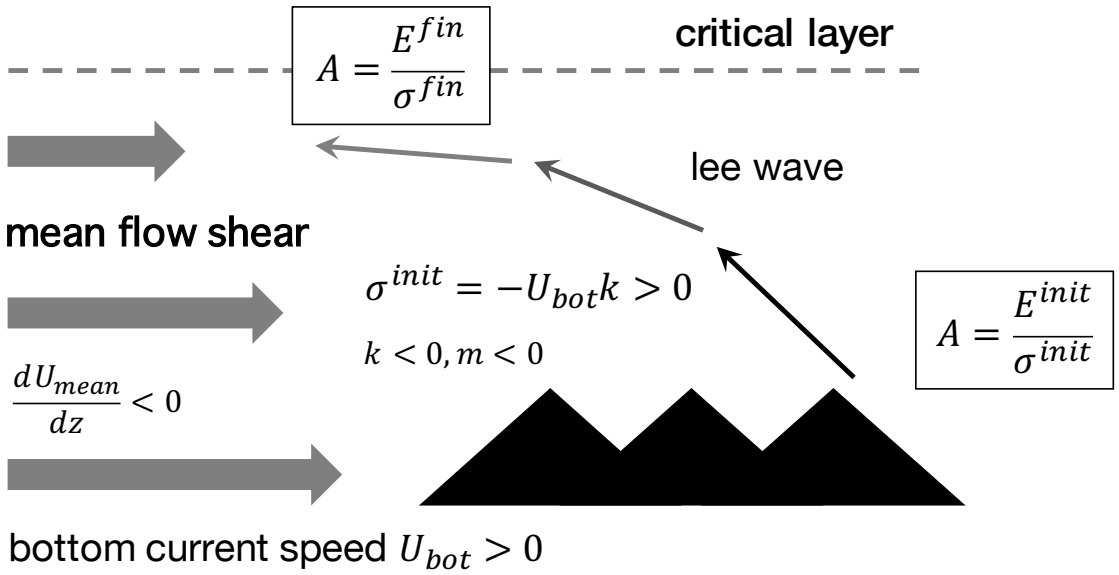

Figure 4.2: Schematic of the evolution of a bottom-generated lee wave packet within the background mean flow shear considered in Waterman et al. (2014).

Chapter 5

General Conclusion

5.1 Summary of this dissertation

The Southern Ocean is a special area where the Antarctic Circumpolar Current (ACC), the bottom-reaching geostrophic flow with vigorous eddies, coexists with the energetic internal waves such as wind-induced near-inertial waves and bottom-generated internal lee waves. Breaking of these internal waves is considered to induce strong turbulent mixing. Although diapycnal mixing in the Southern Ocean has been considered to be potentially important for the meridional overturning circulation (MOC), the number of direct microstructure measurements is too limited to capture the distribution of the diapycnal diffusivity, so that it has been commonly estimated using finescale parameterizations (Henyey et al. 1986; Polzin et al. 1995; Gregg et al. 2003; Ijichi and Hibiya 2015).

However, it was reported that the existing finescale parameterizations tend to overestimate the actual turbulent dissipation rates in the ACC region (Waterman et al. 2013, 2014; Sheen et al. 2013; Takahashi and Hibiya 2019). This suggests that the existing finescale parameterizations, which are formulated on the basis of the wave-wave interaction within the background internal wave field, do not grasp the turbulent mixing processes in the ACC region, where the vigorous geostrophic current including eddies might play an important role in the breaking of internal waves.

In this dissertation, we have aimed to clarify the turbulent mixing processes in the ACC region by investigating why the finescale parameterizations cannot accurately estimate the turbulent dissipation rates.

5.1.1 Assessment of the finescale parameterizations in the ACC region

We have found that the most plausible reason for the overestimating tendency of the finescale parameterizations is that vertical wave number spectrum of the internal wave energy is distorted from the canonical Garrett-Munk (GM) spectrum (Garrett and Munk 1972, 1975; Cairns and Williams 1976) and has a "hump" at lower vertical wave numbers. This hump might be created by near-inertial wave packets and/or internal lee wave packets with low vertical wave numbers superposed on a GM-like internal wave field, which has a flat-shaped vertical wave number energy spectrum (**Chapter 2**).

The eikonal calculations (**Chapter 3**), have suggested that the low vertical wave number internal wave packets constituting the hump might play important roles as the background shear and promote the breaking of high vertical wave number internal wave packets, resulting in enhanced turbulent dissipation rates. However, it has also been suggested that these low vertical wave number internal wave packets hardly cascade down to the turbulent scales because their vertical scales are much larger than the scales of breaking waves.

The finescale parameterizations assume that the background internal wave field has a flat-shaped vertical wave number energy spectrum such as the GM spectrum. Then, the turbulent dissipation rates are estimated from the finescale shear and strain spectral levels, which are calculated by integrating the shear and strain spectra from the lowest wave number to the cut-off wave number. When we apply the finescale parameterizations to the observed velocity profiles, this cut-off wave number is normally set to a smaller value (LADCP-based cut-off wave number) because the shear spectra tend to be contaminated by noise at higher wave numbers. Therefore, the estimated shear and strain spectral levels become much larger than the spectral level at higher wave numbers, which explains the observed bad performance of the finescale parameterizations (**Chapter 3**).

On the other hand, the previous researches (Waterman et al. 2014; Kunze and Lien 2019) theoretically speculated that the wave-mean flow interactions between bottom-

generated internal lee waves and the background mean flow shear might suppress the local turbulent dissipation, causing the overestimation by the finescale parameterizations. Our eikonal calculations, in contrast, have shown that, in the realistic situation where the background mean flow shear and internal wave field coexist, the finescale parameterizations would rather underestimate the actual turbulent dissipation rates (**Chapter 4**). This seems to contradict the relationship confirmed by observations: the overestimates by the finescale parameterizations weakly correlate with the magnitude of background mean flow shear (**Chapter 2**). In our eikonal calculations, the influence of the mean flow shear on the turbulent mixing was strongly dependent on the strength of the WKB scale separation (**Chapter 4**). Therefore, it is suggested that in the real ocean, the background mean flow shear might have little direct effect on turbulent mixing.

5.1.2 The role of geostrophic shear in the breaking of internal waves

From multivariate correlation analyses, it has been suggested that the observed hump in the shear and strain spectra are associated with the geostrophic shear (**Chapter 2).** In the upper ocean, downward-propagating near-inertial wave packets might be generated by wind disturbances and trapped by the geostrophic shear of mesoscale eddies (Kunze 1985). It is also possible that frontal instabilities in the ACC jets spontaneously generate both upward-propagating and downward-propagating near-inertial wave packets (Nagai et al. 2015). In the deep ocean, bottom-reaching geostrophic currents or mesoscale eddies might interact with the small scale rough topography and generate upward-propagating internal lee wave packets. These internal wave packets might create a hump at lower wave numbers in finescale shear and strain spectra, which enhance the local turbulent dissipation rates (**Chapter 3**). Thus, geostrophic shear flows might indirectly promote the breaking of internal waves through enhancement of vertical low wave number internal wave energy.

Previous researches (Waterman et al. 2014; Kunze and Lien 2019) theoretically considered that wave-mean flow interactions between bottom-generated internal lee waves and

the background geostrophic shear flow might suppress the turbulent mixing in the ACC region. However, our eikonal calculations incorporating both the background mean flow shear and the background internal wave field have shown that the mean flow shear rather enhances the turbulent mixing (**Chapter 4**); once again, note that how much the turbulent mixing is enhanced strongly depends on the strength of the WKB scale separation assumed in the eikonal calculations.

5.1.3 Turbulent mixing processes in the ACC region

Figure 5.1 summarizes the conventional (e.g., Waterman et al. 2014) and the new pictures of the turbulent mixing processes in the ACC region. Previously, it has been thought that turbulent mixing primarily caused by the breaking of near-inertial waves and internal lee waves (e.g., Naveira-Garabato et al. 2004). In addition, it has been speculated that the wave-mean flow interaction between these internal wave packets and larger scale geostrophic flows might also play an important role in the turbulent mixing (Waterman et al. 2014; Kunze and Lien 2019).

As a summary of this dissertation, we present a new picture suggested from the results of field observations and eikonal calculations. First of all, turbulent mixing is caused by breaking of high vertical wave number internal waves (**Chapter 3**). Under the vigorous ACC jets, low vertical wave number ($m \sim 0.01$ cpm) near-inertial wave packets and relatively high intrinsic frequency internal lee wave packets create a hump in the finescale shear and strain spectrum (**Chapter 2**), which promote the breaking of high vertical wave number internal waves, resulting in enhanced turbulent mixing (**Chapter 3**). These low vertical wave number internal wave packets might be generated or amplified by large scale geostrophic shear flows (**Chapter 2**).

In eikonal simulations, the initial background internal wave field, for example, an internal wave energy spectrum with a low vertical wave number hump is given a priori as a steady state, but some of the high vertical wave number internal wave energy might

originate from low vertical wave number near-inertial wave and/or internal lee wave energy, which corresponding to the “hump”, cascading down. However, since the GM spectrum is a universal spectrum that has been confirmed even at locations where there is no local internal wave energy forcing, we believe that not all of the high vertical wave number internal wave energy is supplied from the “hump”.

5.1.4 Significance of this study

Since Gregg (1989) proposed the prototype of the finescale parameterizations based on the theoretical model provided by Henyey et al. (1986), several modifications have been made to take into account that the frequency spectrum of internal wave energy is distorted from the canonical GM spectrum. On the other hand, little attention has been paid to the distortion of the vertical wave number spectrum.

In this study, we have pointed out for the first time that the vertical wave number spectrum of internal wave energy is significantly distorted from the GM spectrum in the ACC region, and therefore the existing finescale parameterizations cannot accurately estimate the turbulent dissipation rates. In order to accurately estimate the distribution of diapycnal diffusivity in the ACC region, and probably in the region with vigorous mesoscale eddies, it is necessary to be careful about the vertical wave number band used for the finescale parameterizations.

5.2 Discussions and future works

In this section, we introduce some research related to the results obtained in this dissertation and present our future prospects.

5.2.1 Applicability of the present results to the Kuroshio region

In the midlatitude western boundary current region, such as the Kuroshio region in the western North Pacific, vigorous geostrophic flows accompanying eddies coexist with near-inertial waves generated by wind disturbances under the storm tracks, which might provide strong diapycnal mixing. Furthermore, it has been reported that the Kuroshio and tidal currents can interact with shallow topography with small seamounts, which provides enhanced turbulent dissipation in the Tokara Strait, the East China Sea (Tsutsumi et al. 2017). These features appear to be similar to the turbulent mixing in the Southern Ocean.

There are some studies in which the turbulent dissipation rates in the Kuroshio region were estimated by applying the finescale parameterizations to the vertical profiles of horizontal current speed and/or density (Yang et al. 2014; Jing and Wu 2015). However, the validity of the finescale parameterizations there has not been fully assessed.

Regarding the spectral shape of the internal wave energy in the Kuroshio region, it was reported that downward-propagating near-inertial waves with vertical wave number $m \sim 0.01$ cpm created a pronounced peak in the shear spectrum (Jing and Wu 2015), or downward-propagating near-inertial waves made a spectral enhancement at vertical wave numbers $m < 0.01$ cpm in the shear spectrum (Nagai et al. 2017), both of which are consistent with our findings in the ACC region. However, these spectra were obtained by acoustic Doppler current profilers (ADCP) with no spectral corrections, so that the spectra did not resolve higher wave number shear. Therefore, unfortunately, it cannot be answered at present whether the discussion in this study holds in the Kuroshio region.

5.2.2 Climatology of the background GM-like internal wave spectrum

The finescale parameterizations implicitly assume that the vertical wave number spectrum of internal wave energy is flat like the GM spectrum, which was formulated and has been developed as the empirical curve fit to available observation data. Polzin and Lvov

(2011) reviewed the past available observation data and concluded that the shape of the frequency and vertical wave number spectrum of internal wave energy is geographically variable, though the overall variability tends to be subtle. Unfortunately, they did not refer to the spectra in the Southern Ocean, but they concluded that the deviation is significant in the eastern North Atlantic, Arctic, equator (Eriksen 1985), and near boundaries (Wunsch and Webb 1979).

Quite recently, Eden et al. (2019) numerically evaluated the spectral energy transfers by internal wave-wave interactions for various GM-like energy spectra from the kinematic equation (Hasselmann 1966), and they found that the turbulent dissipation rates (energy transfers to small scales) depend on the spectral slope of the GM-like vertical wave number spectrum. This "slope" seems to be closely related to what we call "hump". In their calculations, as the negative spectral slope increases, the turbulent dissipation rates decrease, which is consistent with our results. Eden et al. (2019) proposed that the existing finescale parameterizations should include the functional dependency on the spectral slope r ($r = 2$ for the GM spectrum, and $r > 2$ for the spectrum with a low wave number hump), which they found from an empirical fit to the results of their evaluation, such as

$$\varepsilon_{fine}^{mod} = (r-1)^{-3}\varepsilon_{fine}, \tag{5.1}$$

where ε_{fine}^{mod} and ε_{fine} indicate the turbulent dissipation rates predicted by the corrected and existing finescale parameterizations, respectively.

In addition, Eden et al. (2019) tried a rough estimate of the global distribution of spectral slope r using density profiles from Argo dataset (Figure 5.2). Here r was obtained by applying a linear-fit to the strain spectra calculated from 200-m-depth bins. The values of r are highly variable both vertically and horizontally, but r is not large in the Southern Ocean. There are several possible reasons: (1) the available data is limited to the upper 2000 m, (2) Eden et al. (2019) focused on the vertical wave number band ($m > 0.005$ cpm) larger than this study, and (3) the contamination of the strain spectra in the sharp

pycnocline (Kunze 2017) might not be removed.

5.2.3 For further improvements of the finescale parameterization

The biggest problem when using the finescale parameterizations in the ACC region is to estimate the turbulent dissipation rate from the shear and strain spectral level of the low vertical wave number band, despite the distorted spectrum. The most simple solution is to use the shear spectra which are free from noise up to the high wave numbers and resolve the Richardson number-based (Ri-based) cut-off wave number m_c^{Ri}, and estimate the spectral levels based on m_c^{Ri}.

However, if noisy velocity profiles such as LADCP data are used, it cannot be determined from the raw data whether the spectrum is distorted or not. In this case, the approach of global mapping of spectral slope, such as that performed by Eden et al. (2019), may help improve the accuracy of the finescale parameterizations. It has some analogy with that if the global distribution of the shear/strain ratio R_ω is known, the turbulent dissipation rate can be estimated only from the Argo float strain data.

The results of our eikonal calculations (**Chapter 3)** have suggested that if the shear spectrum has a large hump, the existing finescale parameterizations with m_c^{Ri} still overestimate the actual turbulent dissipation rates. We have determined m_c^{Ri} empirically based on the spectral integrated inverse Richardson number, but the mechanism by which the spectral roll-off is created should be investigated in the future. For this purpose, we should carry out finestructure and microstructure measurements covering from low vertical wave numbers to high vertical wave numbers in the ACC region or other regions in which the spectral hump is large. In addition, numerical experiments using primitive equations that contain few assumptions are also required.

5.2.4 Implications for parameterizations of internal lee wave-driven mixing in ocean general circulation models

Although the strength and structure of the MOC strongly depend on the global distribution of diapycnal turbulent mixing, the resolution of the existing ocean general circulation models (OGCMs) is too coarse to resolve the small scale turbulent mixing processes and will probably remains to be so even if the computer power will increase in the future. Therefore, in order to reproduce the MOC and the associated long-term climate change, it is necessary to incorporate a diapycnal mixing parameterization for the OGCMs.

Melet et al. (2014) incorporated a parameterization of internal lee-wave driven mixing, which has not been explicitly parameterized in the OGCMs, to an ocean-ice-atmosphere coupled general circulation model to explore its effect on the ocean state. Internal lee wave-driven turbulent dissipation rates were parameterized following the semi-empirical scheme proposed by St. Laurent et al. (2002) originally formulated for internal tide-driven mixing:

$$\varepsilon_L = \frac{q_L E_L(x,y)}{\rho_0} \frac{e^{-z/z_L}}{z_L \left(1 - e^{-H/z_L}\right)}, \tag{5.2}$$

where $\rho_0 = 1035\,\mathrm{kg/m^3}$ is the reference density, q_L is the fraction of the generated internal lee wave energy flux that are dissipated near their generation sites, z_L is the fixed vertical decay scales for the turbulent dissipation rates, $E_L(x,y)$ is the bottom-generated internal lee wave energy flux (Nikurashin and Ferrari 2011), and $H(x,y)$ is the total depth of the ocean. It should be noted that this St. Laurent's scheme deals with turbulent mixing due to the local breaking of high-mode bottom-generated internal waves, so it is completely different from the finescale parameterization, which deals with the energy cascade within the background internal wave spectrum in the interior ocean.

Melet et al. (2014) carried out the main experiment by assuming that the lee wave energy is dissipated locally ($q_L = 1$ and $z_L = 300$ m) because the authors expected that the bottom-generated lee waves might have smaller vertical scales and be dissipated within 10 – 100 km from the generation site by encountering turning points associated with fronts

and eddies of the ACC. However, the results of our study, in which it has been shown that lower vertical wave number internal lee waves might be generated and they takes a long time to break, suggest that q_L (z_L) should be set to a smaller (larger) value, respectively, considering large horizontal advection by the ACC.

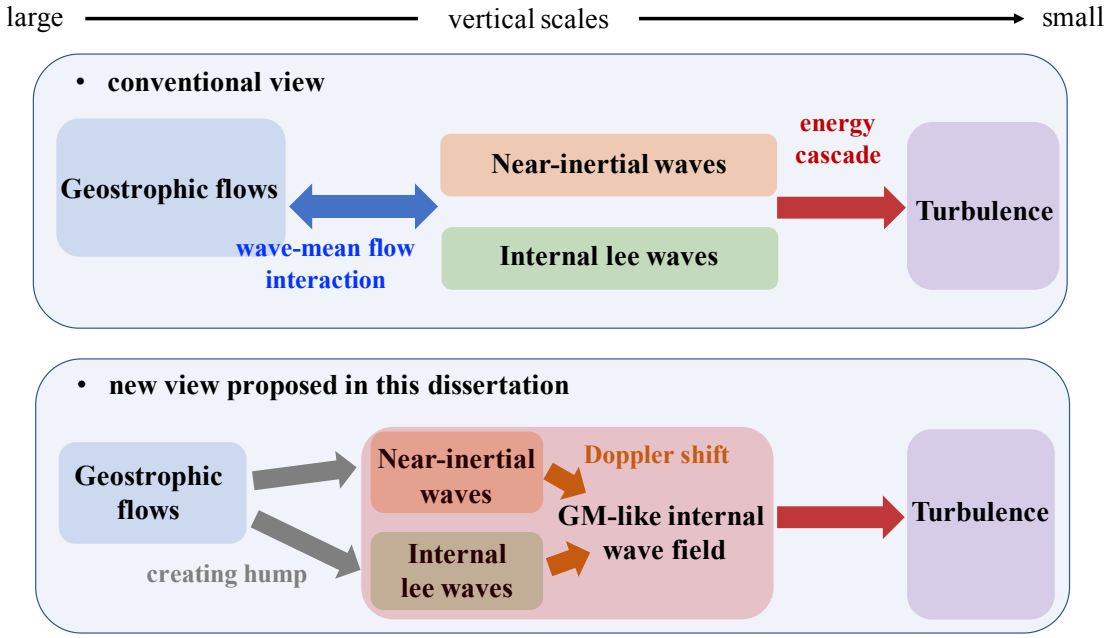

Figure 5.1: Schematic of the turbulent mixing processes in the ACC region. The conventional view (e.g., Waterman et al. 2014) and the new view proposed in this dissertation are compared here.

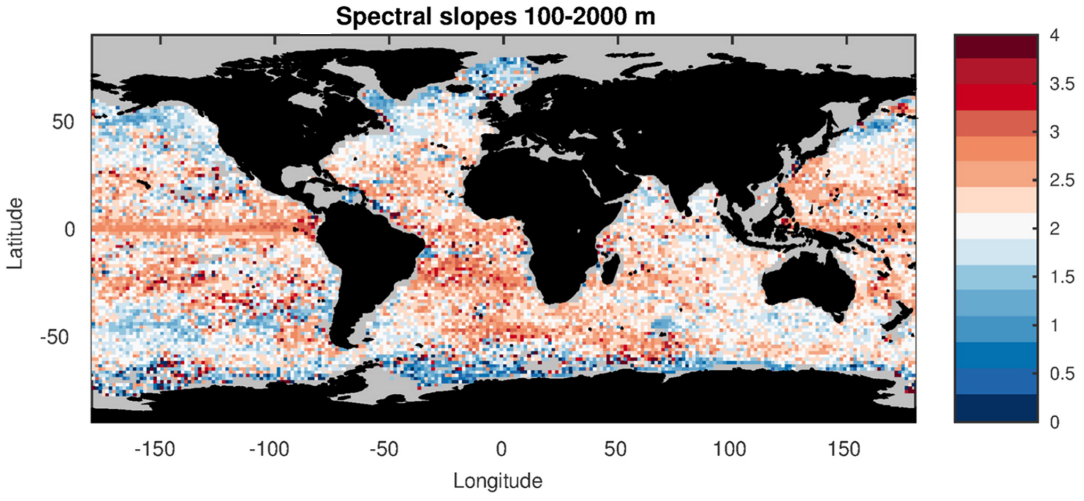

Figure 5.2: Global distribution of spectral slopes of internal waves. The spectral slopes were estimated from linear-fits to vertical wave number spectra of finescale strain obtained from the Argo dataset. Data from 2006 to 2017 were considered. From Eden et al. (2019). **© American Meteorological Society. Used with permission.**

Acknowledgement

First of all, I would like to express my gratitude to my supervisor, Prof. Toshiyuki Hibiya, for his many valuable advices, suggestions, and discussions over the past five years. This work would not have been possible without his continuous support.

My dissertation committee members Profs. Ichiro Yasuda, Akira Oka, Tomoki Tozuka, and Kaoru Sato provided many valuable comments.

I am grateful to the very helpful members and ex-members of the Atmospheric and Oceanic Science Group, Department of Earth and Planetary Science, Graduate School of Science, the University of Tokyo. Special thanks to Drs. Yoshihiro Niwa, Yuki Tanaka, Taira Nagai, Takashi Ijichi, Yohei Onuki, Yukio Masumoto, Tsubasa Kohyama, and Mr. Katsutoshi Fukuzawa for their helpful suggestions. Thanks are also due to Dr. Hiroaki Miura, Dr. Makoto Koike, Dr. Masashi Kohma, Dr. Keiichi Hasunuma, Dr. Shun Ohishi, Dr. Wei Yang, Dr. Tamaki Suematsu, Dr. Yoko Yamagami, Mr. Hajime Ishii, Mr. Ryosuke Yasui, Mr. Shoichiro Kido, Mr. Atsushi Yoshida, Mr. Yuichi Minamihara, Mr. Shuhei Matsugishi, Ms. Emiri Kobori, Mr. Marvin Seow Xiang Ce, Mr. Kazumichi Murata, Mr. Takuro Matsuta, Mr. Takahiro Yanagimachi, Mr. Aiqi Zhang, Ms. Natsumi Tanuma, Ms. Mai Nakazato, Mr. Hidehiro Kusunoki, Mr. Takahiro Kusumi, Mr. Zhang Lianyi, Mr. Yoo-Jun Kim, and Ms. Rika Yoshiyama.

This study benefited from discussions with Drs. Alberto Naveira Garabato, Ren-Chieh Lien, Eric Kunze, Katy Sheen, Michael Gregg, Katsuro Katsumata, Ryuichiro Inoue, Shinya Koketsu, Yutaka Yoshikawa, Naoki Furuichi, Jiro Yoshida, Caitlin Whalen, Eric D'Asaro, Anda Vladoiu, Sebastian Essink, Cimarron Wortham, Jeffley Earley, Friederike Pollmann, Jody Klymak, Kurt Polzin, Robin Robertson, Kelvin Richards, and Robert Pinkel. My gratitude is also extended to Dr. Ryo Furue, Dr. Takahiro Endoh, Dr. Michio Watanabe, Dr. Takao Kawasaki, Dr. Haruka Nakano, Mr. Yasushi Fujiwara, Mr. Yusuke

Ushijima, Mr. Yuki Kita, Ms. Hitomi Oyaizu, Mr. Hung-Wei Chou, and Ms. Akie Sakai.

Observational data are obtained from the 19th and 21st Kaiyodai Antarctic Research Expedition (KARE) surveys, and from the Souther Ocean Finestructure (SOFine) survey. I am deeply grateful to all the participants in the KARE19 and KARE21 cruises of the T/V *Umitaka-maru* of Tokyo University of Marine Science and Technology for their support. Special thanks to Dr. Yujiro Kitade for his valuable suggestions and supports. Observational data from the SOFine survey were kindly provided by Drs. Alberto Naveira Garabato and Alexander Forryan from National Oceanography Centre, University of Southampton.

The basic codes for eikonal calculations (Chapter 3 and 4) were kindly provided by Dr. Takashi Ijichi. The numerical simulations were carried out using the super computer: Fujitsu PRIMERGY CX600M1/CX1640M1(Oakforest-PACS) in the Information Technology Center, the University of Tokyo.

Part of this study was supported by the Research Fellowship of the Japan Society for the Promotion of Science (JSPS).

Finally, I cannot fully express my gratitude to my family, fiancé, and friends for their support and encouragement.

References

Bray, N. A. and N. P. Fofonoff. 1981, Available potential energy for MODE eddies, *Journal of Physical Oceanography*, 11(1):30–47

Bretherton, F. P. and C. Garrett. 1968, Wavetrains in inhomogeneous moving media, *Proceedings of the Royal Society of London. Series A. Mathematical and Physical Sciences*, 302(1471):529–554

Bryan, F. 1987, Parameter sensitivity of primitive equation ocean general circulation models, *Journal of Physical Oceanography*, 17(7):970–985

Cairns, J. L. and G. O. Williams. 1976, Internal wave observations from a midwater float, 2, *Journal of Geophysical Research*, 81(12):1943–1950

Duda, T. F. and C. S. Cox. 1989, Vertical wave number spectra of velocity and shear at small internal wave scales, *Journal of Geophysical Research*, 94(C1):939

Eden, C., F. Pollmann, and D. Olbers. 2019, Numerical evaluation of energy transfers in internal gravity wave spectra of the ocean, *Journal of Physical Oceanography*, 49(3):737–749

Eriksen, C. C. 1985, Some characteristics of internal gravity waves in the equatorial Pacific, *Journal of Geophysical Research*, 90(C4):7243

Fischer, J. and M. Visbeck. 1993, Deep velocity profiling with self-contained ADCPs, *Journal of Atmospheric and Oceanic Technology*, 10(5):764–773

Furuichi, N., T. Hibiya, and Y. Niwa. 2008, Model-predicted distribution of wind-induced internal wave energy in the world's oceans, *Journal of Geophysical Research: Oceans*, 113(9):1–13

REFERENCES

Gargett, A. E., P. J. Hendricks, T. B. Sanford, T. R. Osborn, and A. J. Williams. 1981, A composite spectrum of vertical shear in the upper ocean, *Journal of Physical Oceanography*, 11(9):1258–1271

Garrett, C. and W. Munk. 1972, Space-time scales of internal waves, *Geophysical Fluid Dynamics*, 3(1):225–264

Garrett, C. and W. Munk. 1975, Space-time scales of internal waves: A progress report, *Journal of Geophysical Research*, 80(3):291–297

Gonella, J. 1972, A rotary-component method for analysing meteorological and oceanographic vector time series, *Deep-Sea Research*, 19(12):833–846

Gregg, M. C. 1989, Scaling turbulent dissipation in the thermocline, *Journal of Geophysical Research*, 94(C7):9686–9698

Gregg, M. C., T. B. Sanford, and D. P. Winkel. 2003, Reduced mixing from the breaking of internal waves in equatorial waters, *Nature*, 422(6931):513–515

Gregg, M. C., D. P. Winkel, and T. B. Sanford. 1993, Varieties of fully resolved spectra of vertical shear, *Journal of Physical Oceanography*, 23(1):124–141

Hasselmann, K. 1966, Feynman diagrams and interaction rules of wave-wave scattering processes, *Reviews of Geophysics*, 4(1):1

Henyey, F. S. and N. Pomphrey. 1983, Eikonal description of internal wave interactions: A non-diffusive picture of “ induced diffusion ”, *Dynamics of Atmospheres and Oceans*, 7(4):189–219

Henyey, F. S., J. Wright, and S. M. Flatté. 1986, Energy and action flow through the internal wave field: An eikonal approach, *Journal of Geophysical Research*, 91(C7):8487–8495

REFERENCES

Hibiya, T., N. Furuichi, and R. Robertson. 2012, Assessment of fine-scale parameterizations of turbulent dissipation rates near mixing hotspots in the deep ocean, *Geophysical Research Letters*, 39(24):1–6

Hibiya, T., T. Ijichi, and R. Robertson. 2017, The impacts of ocean bottom roughness and tidal flow amplitude on abyssal mixing, *Journal of Geophysical Research: Oceans*, 122(7):5645–5651

Hibiya, T., M. Nagasawa, and Y. Niwa. 2002, Nonlinear energy transfer within the oceanic internal wave spectrum at mid and high latitudes, *Journal of Geophysical Research*, 107(C11):3207

Hibiya, T., Y. Niwa, K. Nakajima, and N. Suginohara. 1996, Direct numerical simulation of the roll-off range of internal wave shear spectra in the ocean, *Journal of Geophysical Research: Oceans*, 101(C6):14123–14129

Hughes, C. W. 2005, Nonlinear vorticity balance of the Antarctic Circumpolar Current, *Journal of Geophysical Research*, 110(C11):C11008

Ijichi, T. and T. Hibiya. 2015, Frequency-based correction of finescale parameterization of turbulent dissipation in the deep ocean, *Journal of Atmospheric and Oceanic Technology*, 32(8):1526–1535

Ijichi, T. and T. Hibiya. 2017, Eikonal calculations for energy transfer in the deep-ocean internal wave field near mixing hotspots, *Journal of Physical Oceanography*, 47(1):199–210

Iwamae, N., T. Hibiya, and M. Watanabe. 2009, Numerical study of the bottom-intensified tidal mixing using an " eikonal approach ", *Journal of Geophysical Research*, 114(C5):C05022

Jing, Z. and L. Wu. 2015, Intensified diapycnal mixing in the midlatitude western boundary currents, *Scientific Reports*, 4(1):7412

REFERENCES

Kunze, E. 1985, Near-inertial wave propagation in geostrophic shear, *Journal of Physical Oceanography*, 15(5):544–565

Kunze, E. 2017, Internal-wave-driven mixing: Global geography and budgets, *Journal of Physical Oceanography*, 47(6):1325–1345

Kunze, E. and R.-C. Lien. 2019, Energy sinks for lee waves in shear flow, *Journal of Physical Oceanography*, 49(11):2851–2865

Leaman, K. D. and T. B. Sanford. 1975, Vertical energy propagation of inertial waves: A vector spectral analysis of velocity profiles, *Journal of Geophysical Research*, 80(15):1975–1978

Ledwell, J. R., L. C. St. Laurent, J. B. Girton, and J. M. Toole. 2011, Diapycnal mixing in the Antarctic Circumpolar Current, *Journal of Physical Oceanography*, 41(1):241–246

Marshall, J. and K. Speer. 2012, Closure of the meridional overturning circulation through Southern Ocean upwelling, *Nature Geoscience*, 5(3):171–180

McDougall, T. J. and P. Barker. 2011, Getting started with TEOS-10 and the Gibbs Seawater (GSW) Oceanographic Toolbox, Tech. rep., SCOR/IAPSO WG127

Melet, A., R. Hallberg, S. Legg, and M. Nikurashin. 2014, Sensitivity of the ocean state to lee wave − driven mixing, *Journal of Physical Oceanography*, 44(3):900–921

Meyer, A., K. L. Polzin, B. M. Sloyan, and H. E. Phillips. 2016, Internal waves and mixing near the Kerguelen Plateau, *Journal of Physical Oceanography*, 46(2):417–437

Meyer, A., B. M. Sloyan, K. L. Polzin, H. E. Phillips, and N. L. Bindoff. 2015, Mixing variability in the Southern Ocean, *Journal of Physical Oceanography*, 45(4):966–987

Munk, W. 1981, Internal waves and small-scale processes, in Evolution of Physical Oceanography, edited by B. A. Warren and C. Wunsch, pp. 264–291, MIT Press, Cambridge

REFERENCES

Munk, W. and C. Wunsch. 1998, Abyssal recipes II: Energetics of tidal and wind mixing, *Deep Sea Research Part I: Oceanographic Research Papers*, 45(12):1977–2010

Nagai, T., D. Hasegawa, T. Tanaka, H. Nakamura, E. Tsutsumi, R. Inoue, and T. Yamashiro. 2017, First evidence of coherent bands of strong turbulent layers associated with high-wavenumber internal-wave shear in the upstream Kuroshio, *Scientific Reports*, 7(1):14555

Nagai, T., A. Tandon, E. Kunze, and A. Mahadevan. 2015, Spontaneous generation of near-inertial waves by the Kuroshio front, *Journal of Physical Oceanography*, 45(9):2381–2406

Nagasawa, M., T. Hibiya, K. Yokota, Y. Tanaka, and S. Takagi. 2007, Microstructure measurements in the mid-depth waters of the North Pacific, *Geophysical Research Letters*, 34(5):1–5

Nasmyth, P. W. 1970, Oceanic turbulence, Ph.D. thesis, University of British Columbia

Naveira-Garabato, A. C., K. L. Polzin, B. A. King, K. J. Heywood, and M. Visbeck. 2004, Widespread intense turbulent mixing in the Southern Ocean, *Science*, 303(5655):210–213

Nikurashin, M. and R. Ferrari. 2010, Radiation and dissipation of internal waves generated by geostrophic motions impinging on small-scale topography: Application to the Southern Ocean, *Journal of Physical Oceanography*, 40(9):2025–2042

Nikurashin, M. and R. Ferrari. 2011, Global energy conversion rate from geostrophic flows into internal lee waves in the deep ocean, *Geophysical Research Letters*, 38(8):1–6

Nikurashin, M., G. K. Vallis, and A. Adcroft. 2013, Routes to energy dissipation for geostrophic flows in the Southern Ocean, *Nature Geoscience*, 6(1):48–51

REFERENCES

Niwa, Y. and T. Hibiya. 2011, Estimation of baroclinic tide energy available for deep ocean mixing based on three-dimensional global numerical simulations, *Journal of Oceanography*, 67(4):493–502

Oakey, N. S. 1982, Determination of the rate of dissipation of turbulent energy from simultaneous temperature and velocity shear microstructure measurements, *Journal of Physical Oceanography*, 12(3):256–271

Olbers, D., D. Borowski, C. Völker, and J.-o. Wölff. 2004, The dynamical balance, transport and circulation of the Antarctic Circumpolar Current, *Antarctic Science*, 16(4):439–470

Olbers, D. and M. Visbeck. 2005, A model of the zonally averaged stratification and overturning in the Southern Ocean, *Journal of Physical Oceanography*, 35(7):1190–1205

Osborn, T. R. 1980, Estimates of the local rate of vertical diffusion from dissipation measurements, *Journal of Physical Oceanography*, 10(1):83–89

Polzin, K., E. Kunze, J. Hummon, and E. Firing. 2002, The finescale response of lowered ADCP velocity profiles, *Journal of Atmospheric and Oceanic Technology*, 19(2):205–224

Polzin, K. L. and Y. V. Lvov. 2011, Toward regional characterizations of the oceanic internal wavefield, *Reviews of Geophysics*, 49(4):1–61

Polzin, K. L., J. M. Toole, and R. W. Schmitt. 1995, Finescale parameterizations of turbulent dissipation, *Journal of Physical Oceanography*, 25(3):306–328

Rimac, A., J. Storch, C. Eden, and H. Haak. 2013, The influence of high ‐ resolution wind stress field on the power input to near ‐ inertial motions in the ocean, *Geophysical Research Letters*, 40(18):4882–4886

REFERENCES

Rintoul, S. R. 2018, The global influence of localized dynamics in the Southern Ocean, *Nature*, 558(7709):209–218

Shang, X., Y. Qi, G. Chen, C. Liang, R. G. Lueck, B. Prairie, and H. Li. 2017, An expendable microstructure profiler for deep ocean measurements, *Journal of Atmospheric and Oceanic Technology*, 34(1):153–165

Sheen, K. L., J. A. Brearley, A. C. Naveira Garabato, D. A. Smeed, S. Waterman, J. R. Ledwell, M. P. Meredith, L. St. Laurent, A. M. Thurnherr, J. M. Toole, and A. J. Watson. 2013, Rates and mechanisms of turbulent dissipation and mixing in the Southern Ocean: Results from the Diapycnal and Isopycnal Mixing Experiment in the Southern Ocean (DIMES), *Journal of Geophysical Research: Oceans*, 118(6):2774–2792

Speer, K., S. R. Rintoul, and B. Sloyan. 2000, The diabatic Deacon cell, *Journal of Physical Oceanography*, 30(12):3212–3222

St. Laurent, L., A. C. Naveira Garabato, J. R. Ledwell, A. M. Thurnherr, J. M. Toole, and A. J. Watson. 2012, Turbulence and diapycnal mixing in Drake Passage, *Journal of Physical Oceanography*, 42(12):2143–2152

St. Laurent, L. C., H. L. Simmons, and S. R. Jayne. 2002, Estimating tidally driven mixing in the deep ocean, *Geophysical Research Letters*, 29(23):21–1–21–4

Takahashi, A. and T. Hibiya. 2019, Assessment of finescale parameterizations of deep ocean mixing in the presence of geostrophic current shear: Results of microstructure measurements in the Antarctic Circumpolar Current region, *Journal of Geophysical Research: Oceans*, 124(1):135–153

Thurnherr, A. 2011, How to process LADCP data with the LDEO software, Tech. rep.

Thurnherr, A. M. 2012, The finescale response of lowered ADCP velocity measurements processed with different methods, *Journal of Atmospheric and Oceanic Technology*, 29(4):597–600

REFERENCES

Tsujino, H., H. Hasumi, and N. Suginohara. 2000, Deep pacific circulation controlled by vertical diffusivity at the lower thermocline depths, *Journal of Physical Oceanography*, 30(11):2853–2865

Tsutsumi, E., T. Matsuno, R.-C. Lien, H. Nakamura, T. Senjyu, and X. Guo. 2017, Turbulent mixing within the Kuroshio in the Tokara Strait, *Journal of Geophysical Research: Oceans*, 122(9):7082–7094

Visbeck, M. 2002, Deep velocity profiling using lowered acoustic Doppler current profilers: Bottom track and inverse solutions, *Journal of Atmospheric and Oceanic Technology*, 19(5):794–807

Watanabe, M. and T. Hibiya. 2005, Estimates of energy dissipation rates in the three-dimensional deep ocean internal wave field, *Journal of Oceanography*, 61(1):123–127

Waterman, S., A. Naveira Garabato, and K. Polzin. 2013, Internal waves and turbulence in the Antarctic Circumpolar Current, *Journal of Physical Oceanography*, 43(2):259–282

Waterman, S., K. L. Polzin, A. C. Naveira Garabato, K. L. Sheen, and A. Forryan. 2014, Suppression of internal wave breaking in the Antarctic Circumpolar Current near topography, *Journal of Physical Oceanography*, 44(5):1466–1492

Webb, D. J. and N. Suginohara. 2001, Vertical mixing in the ocean, *Nature*, 409(6816):37–37

Whalen, C. B., L. D. Talley, and J. A. MacKinnon. 2012, Spatial and temporal variability of global ocean mixing inferred from Argo profiles, *Geophysical Research Letters*, 39(18)

Wijesekera, H., L. Padman, T. Dillon, M. Levine, C. Paulson, and R. Pinkel. 1993, The application of internal-wave dissipation models to a region of strong mixing, *Journal of Physical Oceanography*, 23(2):269–286

REFERENCES

Wu, L. X., Z. Jing, S. Riser, and M. Visbeck. 2011, Seasonal and spatial variations of Southern Ocean diapycnal mixing from Argo profiling floats, *Nature Geoscience*, 4(6):363–366

Wunsch, C. and S. Webb. 1979, The climatology of deep ocean internal waves, *Journal of Physical Oceanography*, 9(2):235–243

Yang, Q., W. Zhao, M. Li, and J. Tian. 2014, Spatial structure of turbulent mixing in the Northwestern Pacific Ocean, *Journal of Physical Oceanography*, 44(8):2235–2247